The non-steroidal mineralocorticoid receptor (MR) antagonist (FINERENONE) reverses Western diet-induced kidney disease by enhancing mitochondrial metabolism and decreasing lipid accumulation and inflammation

Komuraiah Myakala[1], Xiaoxin X Wang[1], Nataliia Shults[1,3], Eleni P. Hughes[1], Patricia de Carvalho Ribeiro[1], Rozhin Penjweini[4], Katie Link[4], Keely Barton[1], Bryce Jones[1,2], Ewa Krawczyk[1,3], Cheryl Clarkson Paredes[6], Anastas Popratiloff[6], Jay R. Knutson[4], Ashley L Cowart[5], Moshe Levi[1,7]

[1]Department of Biochemistry and Molecular & Cellular Biology, Georgetown University, Washington, DC, USA
[2]Department of Pharmacology and Physiology, Georgetown University, Washington, DC, USA
[3]Department of Pathology, Georgetown University, Washington, DC, USA
[4]Advanced Microscopy and Biophotonics, NHLBI, NIH, Bethesda MD
[5]Department of Biochemistry and Molecular & Cellular Biology, Virginia Commonwealth University, Richmond, VA
[6]GW Nanofabrication and Imaging Center (GWNIC), George Washington University, Washington DC
[7]Center for Biomedical and Biological Engineering, Georgetown, Washington DC, USA

Keywords: Diet-induced obesity, mineralocorticoid receptor, mitochondrial metabolism, estrogen-related receptor, lipid accumulation, renal inflammation, renal fibrosis.

Correspondence: Moshe Levi, MD. Georgetown University, Department of Biochemistry and Molecular & Cellular Biology, 3900 Reservoir Road, Basic Science 353, Washington, DC 20007. Email: Moshe.Levi@georgetown.edu

ABSTRACT

Mineralocorticoid receptor (MR) overactivation plays a crucial role in the pathogenesis of chronic kidney disease, as well as several cardiovascular and arterial diseases. Current studies determined the mechanisms of the beneficial kidney effects of the non-steroidal MR antagonist finerenone (FN) in a mouse model of western diet-induced obesity and insulin resistance. 10-week-old male C57BL/6J mice were fed a low fat (LF) or western diet (WD) for 12 weeks followed by treatment with either vehicle or finerenone (FN) for another 14 weeks (intervention studies) until they were 36 weeks old. Finerenone treatment prevented a) the increased albuminuria and kidney injury molecule 1 (KIM1), b) the expanded extracellular mesangial matrix, podocyte loss, and renal, c) fibronectin, collagen IV , CD45 and CD68 immunostaining, d) glomerular basement membrane disruption, podocyte foot process loss, and mitochondrial structural abnormalities, e) pro-inflammatory cytokines (MCP1), innate immunity pathways (TLR2, STING, STAT3), and fibrosis marker fibronectin, TGFβ and Pai1, and f) increased kidney cholesterol levels. There was also reduced expression of nuclear receptors ERRγ without changes in ERRα in WD-fed mice whereas both ERRα and ERRγ expression levels increased markedly with finerenone. NADH lifetime analysis showed decreased bound NADH, compatible with decreased mitochondrial OXPHOS in the kidneys of WD-fed mice compared to controls, which was prevented by finerenone treatment. In conclusion, finerenone treatment exhibits a renal protective role and prevents the progression of kidney disease by regulating mitochondrial function, most likely via ERRγ and reducing lipid accumulation and inflammation.

INTRODUCTION

Chronic kidney disease (CKD) affects approximately 850 million people worldwide, with 3.9 million requiring kidney replacement (1). Up to 40% of people with diabetes develop CKD, making diabetic kidney disease (DKD) the leading cause of kidney failure globally (2). The increasing prevalence of type 2 diabetes (T2D) has significantly raised the rate of CKD diagnoses. Individuals diagnosed with both conditions face a substantially higher risk of mortality, often experiencing a three-fold increase compared to those with only T2D (3, 4). Additionally, cardiovascular mortality in CKD stage 3 exceeds the risk of kidney failure by tenfold, positioning CKD as the fifth leading cause of death globally by 2040, primarily due to its association with T2D (5-7).

Several factors, such as obesity, hypertension, and insulin resistance, are recognized as critical risk determinants for chronic kidney disease (CKD) and cardiovascular complications, even without diabetes or hyperglycemia (8-11). These conditions promote systemic inflammation, oxidative stress, and endothelial dysfunction, driving renal and cardiovascular damage (9, 11-13). Angiotensin-converting enzyme inhibitors (ACE inhibitors) and angiotensin receptor blockers (ARBs) have been important in managing albuminuric CKD for over two decades (14, 15). These agents mitigate the progression of CKD by inhibiting the renin-angiotensin system, thereby reducing intraglomerular pressure and proteinuria. Their efficacy in slowing CKD progression and reducing cardiovascular events has been documented in landmark trials (14-16).

While renin-angiotensin system (RAS) blockers such as angiotensin-converting enzyme inhibitors (ACEis) and angiotensin receptor blockers (ARBs) offer significant kidney

protection, a substantial risk of chronic kidney disease (CKD) and cardiovascular disease progression persists. Attempts to enhance therapeutic outcomes through dual RAS blockade combining ACEis, ARBs, or direct renin inhibitors have been largely unsuccessful due to increased risks of adverse events (17-20). Like ACEis and ARBs, SGLT2 inhibitors are another class of medications that have demonstrated significant benefits in managing CKD, both in patients with and without diabetes. They prevent CKD progression by reducing glomerular hypertension through tubuloglomerular feedback, independent of glycemic control. Clinical trials, such as EMPA-KIDNEY, and seminal randomized controlled trials like CREDENCE and DAPA-CKD, have highlighted their efficacy in slowing eGFR decline, reducing albuminuria, and improving cardiovascular and renal outcomes (21). GLP-1 receptor agonists have also been associated with lower all-cause mortality and lower sepsis- and infection-related mortality in patients with diabetes and advanced CKD or ESKD (22).

Interestingly, the mineralocorticoid receptor (MR) plays a key role in the aldosterone-sensitive distal nephron, regulating sodium (Na^+) and potassium (K^+) homeostasis, extracellular fluid volume, and blood pressure (23-27). Aldosterone secretion is primarily stimulated by elevated blood K^+ levels or activation of the renin-angiotensin-aldosterone system (RAAS) due to reduced blood volume or sodium intake. By forming a complex with MR in principal distal nephron cells, aldosterone enhances Na^+ reabsorption and K^+ excretion through the activation of epithelial sodium channels (ENaC) and Na^+–K^+ ATPase (28, 29). In intercalated cells, the aldosterone-MR complex upregulates pendrin to increase chloride (Cl^-) reabsorption and decrease K^+ secretion, while in distal convoluted tubule cells, it boosts Na^+ and Cl^- reabsorption by enhancing sodium–chloride

cotransporter (NCC) activity. Overactivation of the MR in animal models of chronic kidney disease (CKD) has been shown to exacerbate sodium retention and hypertension, while simultaneously driving pathological processes such as inflammation and fibrosis within the kidneys, vasculature, and heart (24, 30-32). These maladaptive responses contribute significantly to the progression of cardiorenal disease, a condition characterized by the interplay of kidney and cardiovascular dysfunction. The resulting tissue damage and systemic effects underscore the pivotal role of MR signaling in disease pathogenesis. Therapeutically, targeting MR overactivation presents a compelling strategy to mitigate CKD progression and its associated cardiovascular complications (26, 27, 33, 34). MR antagonism not only reduces sodium retention and blood pressure but also attenuates inflammatory and fibrotic pathways, offering dual benefits in preserving renal function and improving cardiovascular outcomes. By addressing both renal and cardiac damage, MR blockade holds the potential to significantly lower morbidity and mortality in patients with CKD, making it a critical focus in the development of novel cardiorenal therapies (26, 27, 33, 34). The pressing need for therapies to effectively slow the progression of cardiorenal disease with improved safety profiles has driven substantial efforts toward the development of nonsteroidal mineralocorticoid receptor antagonists (MRAs) (25-27, 35-40). Recent development and meta-analysis studies demonstrated that the combination of MRAs and SGLT2 inhibitors resulted in greater reductions in albuminuria and blood pressure compared to SGLT2 inhibitors alone, clearly demonstrating the promising role of MRAs in providing renal benefits (41). Finerenone, a novel nonsteroidal MRA, stands out due to its unique binding characteristics, which confer high potency and selectivity for the MR. Preclinical studies have demonstrated that finerenone exerts anti-inflammatory,

antifibrotic, and antiproliferative effects, contributing to the modulation of pathological tissue remodeling in both the heart and kidneys (29, 31, 38, 39, 42-46). Clinical evidence supports finerenone's efficacy and safety. Phase II trials reported dose-dependent reductions in albuminuria with a safety profile comparable to placebo, while also showing smaller increases in serum potassium levels relative to spironolactone (29). Furthermore, in a pivotal Phase III trial involving patients with CKD and type 2 diabetes mellitus (T2DM), finerenone significantly improved long-term kidney and cardiovascular outcomes compared to placebo (44). These findings highlight finerenone's potential as a transformative therapy for managing CKD and associated cardiovascular risks, addressing a critical unmet need in this patient population.

Obesity is a well-established and potent risk factor for the development and progression of kidney disease. It significantly elevates the risk of major contributing conditions to chronic kidney disease (CKD), including diabetes mellitus and hypertension, both of which are leading causes of CKD worldwide. Additionally, obesity exerts direct deleterious effects on renal structure and function, independent of these comorbidities. Western diets containing high amounts of saturated fat are major contributors to obesity, acting as metabolic stressors that further aggravate CKD. In the context of diabetic kidney disease (DKD), the Western-type diet worsens metabolic stress by promoting insulin resistance, hyperglycemia, and lipid accumulation, further aggravating DKD progression (47, 48). These factors disrupt the glomerular filtration barrier, leading to proteinuria, a key marker and driver of DKD. Together, these mechanisms accelerate DKD progression and heighten cardiovascular and renal risks.

The renal estrogen-related receptor gamma (ERRγ) pathway is a critical regulator of kidney function, particularly in the context of energy metabolism, oxidative stress, and fibrotic responses. ERRγ plays key roles in the transcriptional regulation of genes involved in mitochondrial function, lipid metabolism, and cellular homeostasis.

While mineralocorticoid receptor (MR) antagonists have shown promise in managing cardiorenal diseases, the specific efficacy and mechanisms of finerenone under conditions of a western diet-induced obesity and insulin resistance remain insufficiently understood.

MATERIALS AND METHODS

Animal study

Ten-week-old male C57BL/6J mice were procured from the Jackson Laboratory and housed under standard conditions with a 12-hour light/12-hour dark cycle. Mice were fed either a western diet (WD: 42% milkfat, 34% sucrose, and 0.2% cholesterol; Research Diet, D12079B) or a matched low-fat control diet (LFD: 10 kcal % fat; Research Diet, D14042701) for a duration of 12 weeks. Following this period, the low-fat and western diet-fed mice were randomly assigned to one of four groups: (1) low-fat diet (LF), (2) low-fat diet supplemented with 10 mg/kg of finerenone (LF + FN), (3) Western diet (WD), and (4) western diet supplemented with 10 mg/kg of finerenone (WD + FN). These dietary regimens were maintained for an additional 14 weeks. Food intake and body weight were monitored biweekly throughout the study.

Before the termination of the study, mice were placed in metabolic cages for 24-hour urine collection. Urine samples were analyzed for volume, creatinine, albumin, kidney injury molecule-1 (KIM-1), neutrophil gelatinase-associated lipocalin (NGAL), and thiobarbituric acid reactive substances (TBARS) as previously described (49, 50).

At the end of the study, mice were euthanized via CO_2 inhalation, and blood samples were collected by cardiac puncture for the measurement of glucose, triglycerides, and cholesterol levels. Kidneys were harvested immediately and processed as follows: (a) snap-frozen for RNA extraction, western blotting, and lipid analysis; (b) fixed in 10% formalin for histological evaluation; and (c) embedded in OCT for immunofluorescence microscopy as per standard lab protocols (51, 52). Animal experiments were approved by the Institutional Animal Care and Use Committees at the Department of Comparative

Medicine and the Institutional Animal Care and Use Committee (IACUC) at Georgetown University and followed the standards set by National Institute of Health (NIH) guidelines.

Biochemical Analysis

Fasting blood glucose levels were measured using a glucometer (Elite XL; Bayer, Tarrytown, NY, USA). Plasma triglycerides and cholesterol levels were quantified with commercially available kits (Catalog #23666410 and #23666202, Pointe Scientific, USA). Urine albumin and creatinine concentrations were assessed using kits from Exocell (Philadelphia, PA, USA) and BioAssay Systems (Hayward, CA, USA), respectively. Urinary thiobarbituric acid reactive substances (TBARS) were measured using the Quantichrom TBARS Assay Kit (BioAssay Systems, Hayward, CA, USA). Urinary kidney injury molecule-1 (KIM-1; Catalog #ab213477) and neutrophil gelatinase-associated lipocalin (NGAL; Catalog #ab199083) concentrations were determined using mouse enzyme-linked immunosorbent assay (ELISA) kits (Abcam, Cambridge, MA, USA). All the assays were done according to the manufacturer's instructions (51, 52).

Blood Pressure Measurement

Systolic blood pressure (SBP) was measured using the tail-cuff method (Model BP-2000-M-6, Visitech Systems, Apex, NC, USA) as previously described (53). Briefly, mice were acclimated to the procedure over two days before data collection. Measurements were recorded over several cycles, and mean SBP values were calculated from at least 25–30 measurements per animal at each time point.

Real-Time Quantitative PCR (qPCR)

Total RNA was isolated from snap-frozen kidney tissue using the NucleoSpin RNA kit (Takara Bio, Germany). Complementary DNA (cDNA) was synthesized using a high-capacity cDNA reverse transcription kit (Applied Biosystems, USA) following the manufacturer's instructions. Quantitative real-time PCR (qPCR) was performed as previously described, with target gene expression normalized to 18S rRNA levels (51, 52). Primer sequences are provided in Supplemental Table 1.

Immunoblotting

Kidney tissues (25 mg) were homogenized in T-PER buffer (Thermo Scientific, Catalog #78510) supplemented with protease and phosphatase inhibitors. Total protein concentration was determined using the BCA assay (Thermo Fisher Scientific). Equal amounts of protein were separated on SDS-PAGE gels, transferred onto PVDF membranes, and probed with primary antibodies including fibronectin (Catalog #SAB5700724, Sigma; 1:1000 dilution) and β-actin (Catalog #A5316, Sigma-Aldrich; 1:5000 dilution). Immune complexes were detected with HRP-conjugated secondary antibodies and visualized using the Azure C300 digital imager (Azure Biosystems, Dublin, CA, USA). Densitometry was performed using Fiji ImageJ software (51, 52).

Histology Staining

Paraffin-embedded kidney tissue sections (5 µm thick) were stained with Periodic Acid-Schiff (PAS) and Picrosirius Red (PSR) following standard protocols performed by the shared resources core facility at Georgetown University (51, 52). Images were captured

using a high-capacity digital slide scanner (Aperio ScanScope GT450, Leica Microsystems, Germany). PSR-stained slides were visualized under polarized light and imaged using an IX83 Inverted Microscope (Olympus, Tokyo, Japan). The glomerular mesangial expansion was quantified as the PAS-positive, nucleus-free mesangial area using the ScanScope image analyzer. PSR images were analyzed in Fiji ImageJ, and data were presented as the percentage of positive-stained pixels.

Immunofluorescence Microscopy

Frozen kidney sections (5 µm thick) were used for Oil-Red-O staining to detect neutral lipid (cholesterol esters and triglycerides) accumulation and for immunostaining. Sections were stained with antibodies against fibronectin (SAB5700724, Sigma), type IV collagen (SAB4500375, Sigma), and synaptopodin (SAB3500586, Sigma). Imaging was performed using a confocal microscope (Leica SP8, Germany). Quantification of the positive staining area in the glomerular region was conducted in Fiji ImageJ, as described previously (51, 52).

Liquid Chromatography–Mass Spectrometry (LC-MS)

Approximately 20–25 mg of frozen kidney tissue was homogenized in methanol and extracted using methanol: chloroform mixture (2:1 ratio) with 10 µL of an internal sphingolipid standard. Samples were incubated overnight and centrifuged. The supernatant evaporated, and the lipid residue was resuspended in methanol: water (1:1 ratio) before injection. Samples were analyzed using the AB Sciex 5500 QTrap system (GenTech Scientific). Relative ceramide levels were quantified using high-performance

liquid chromatography-tandem mass spectrometry (HPLC-MS/MS) and normalized to tissue weight.

Electron Microscopy

Renal cortex tissues were fixed in the 2.5% glutaraldehyde/2%paraformaldehyde/ 0.05 mol/L cacodylate solution, post-fixed with 1% osmium tetroxide, and embedded in EmBed812. For *transmission electron microscopy* (TEM) imaging acquisition, ultrathin sections (70 nm) were poststained with uranyl acetate and lead citrate and examined in the Talos F200X FEG TEM (FEI, Hillsboro, OR) at 80 kV located at the George Washington University Nanofabrication and Imaging Center. Digital electron micrographs were recorded with the TIA software (FEI). For *scanning electron microscopy (SEM)* evaluation, ultrathin sections (120 nm) were mounted in silicon wafers and observed with a Teneo LV FEG SEM (FEI, ThermoFischer Scientific). For optimal results, we used the optiplan mode (high-resolution) equipped with an in-lens T1 detector (Segmented A+B, working distance of 8 mm). Low-magnification images (600×) were first taken for the observation then we performed high magnification tile images of our regions of interest (35,000) using 2 kV and 0.4 current landing voltage.

Morphometric analysis was performed under blinded conditions by systematic uniform random sampling with the Fiji Software using 20 randomly selected images. In EM images, the volume fraction of mitochondria was determined using the morphometric technique with a dot grid. The size of each mitochondrion was calculated by using the FIJI ImageJ software. Mitochondrial types were determined using the point counting method (54).

Fluorescence Lifetime Imaging Microscopy (FLIM)

Two-photon FLIM was performed using an Olympus IX81/FV1000 confocal microscope equipped with a Mai Tai BB DeepSee femtosecond laser (Spectra-Physics, Santa Clara, CA, USA). Kidney sections were excited with a wavelength of 740 nm, and emission was detected with a PMC100 air-cooled detector. Time-correlated single-photon counting (TCSPC) histograms were constructed, and FLIM images were analyzed using SPSS 14.0 (IBM, Chicago, IL, USA) (55). Statistical significance was defined as $p < 0.05$.

Mitochondrial Complex Activity Assay

Mitochondrial fractions were isolated from frozen kidney tissue as described (56) previously (56). Complex I (NADH dehydrogenase; Catalog # ab109729) and complex IV (cytochrome c oxidase; Catalog # ab109911) activities were measured using assay kits from Abcam (USA) according to the manufacturer's protocols.

Statistical Analysis

Data are presented as mean ± standard error. Comparisons between groups were analyzed using a one-way analysis of variance (ANOVA) followed by a Student-Newman-Keuls post hoc test (GraphPad Prism 8, GraphPad Software, Inc., La Jolla, CA, USA). A p-value of <0.05 was considered statistically significant.

RESULTS

Effects of finerenone treatment on metabolic and biochemical characteristics in western diet fed mice

Ten-week-old male C57BL/6J mice were fed either a low-fat (LF) or Western diet (WD) for 12 weeks. Following this period, the mice were maintained on their respective diets, with or without finerenone supplementation, for an additional 14 weeks. Food intake and body weight were recorded every two weeks throughout the study (Supplementary Fig. 1). WD-fed mice consumed more food than LF-fed mice, while finerenone supplementation did not affect food intake compared to diet-matched controls (Supplementary Fig. 1). Consistent with the increased caloric intake, WD-fed mice showed significant weight gain compared to LF-fed controls. However, body weight in either dietary group was unaffected by finerenone treatment. Fasting blood glucose levels were similar among the four groups. Plasma triglyceride and cholesterol levels, which were markedly elevated in WD-fed mice at 36 weeks of age, were significantly reduced with finerenone treatment (Table 1). Systolic blood pressure did not differ significantly across any of the groups.

Finerenone treatment protects the renal injury in a western diet-induced obesity mouse model

At the end of the finerenone treatment, 24-hour urine samples were collected to assess glomerular filtration barrier function and tubular injury. Urinary albumin levels served as an indicator of glomerular injury, while kidney injury molecule-1 (KIM1) and lipocalin-2 (NGAL) were measured to evaluate tubular damage. Western diet (WD)-fed mice showed a significant increase in urinary albumin, KIM1/creatinine ratio, and NGAL compared to

low-fat (LF) fed controls. However, finerenone supplementation markedly reduced these levels in WD-fed mice (Fig. 1A-B). Additionally, WD-fed mice demonstrated increased thiobarbituric acid reactive substances (TBARS), a marker of lipid peroxidation, which was significantly lowered following finerenone treatment (Fig. 1C).

Diet-induced obesity commonly leads to kidney pathology characterized by increased mesangial matrix accumulation, foot process effacement, and thickening of the glomerular basement membrane (GBM), culminating in renal fibrosis (57). To evaluate how WD-induced obesity and insulin resistance affect renal histopathology, periodic acid–Schiff (PAS) and picrosirius red (PSR) staining were performed on kidney sections. In PAS-stained tissues, WD-fed mice exhibited pronounced mesangial expansion compared to LF-fed mice, whereas finerenone treatment significantly reduced mesangial enlargement in WD-fed animals (Fig. 2A). Immunofluorescence staining for synaptopodin, a marker of podocyte integrity, revealed a notable decrease in WD-fed mice compared to LF-fed controls; finerenone intervention preserved synaptopodin expression and thereby mitigated podocyte damage (Fig. 2B).

Electron microscopy was then employed to examine ultrastructural changes in the GBM and podocyte foot processes. Scanning electron microscopy (SEM) revealed GBM thickening in WD-fed mice, which was alleviated by finerenone supplementation (Fig. 2C). Moreover, WD-fed mice exhibited severe podocyte foot process effacement (including widening, fusion, and loss of slit diaphragms), but these abnormalities were prevented by finerenone (Fig. 2D). Consistent with prior reports indicating that mineralocorticoid receptor inhibition safeguards the endothelial glycocalyx in diabetic conditions (58), transmission electron microscopy (TEM) revealed significantly reduced glycocalyx

thickness in WD-fed mice, an effect that was reversed by finerenone (Fig. 2E). Higher magnification TEM images further demonstrated decreased glycocalyx density and distribution in WD-fed mice, alterations that were similarly restored by finerenone (Fig. 2F). Collectively, these results demonstrate that finerenone significantly ameliorates WD-induced kidney damage, preserving both functional and structural integrity in the glomerulus and tubules.

Finerenone treatment ameliorated renal fibrosis in western diet-induced obese mice

The accumulation of fibrillary collagens within the renal tubular interstitium is a well-documented feature in mice fed a high-fat diet (19, 59, 60). Picrosirius red (PSR) staining, followed by polarized light imaging and subsequent quantification, revealed elevated fibrillary collagen deposition in the tubular interstitial space of WD-fed kidneys compared to LF-fed controls. This increase was attenuated by finerenone treatment (Fig. 3A–C). Immunofluorescence staining for fibronectin and collagen type IV both key extracellular matrix components produced by mesangial cells that contribute to glomerulosclerosis showed significantly higher accumulation in WD-fed mice compared to LF-fed mice. However, finerenone administration prevented these increases (Fig. 3D-3E). Consistent with these findings, both RT-qPCR and western blot analyses revealed upregulated fibronectin transcript and protein levels in WD-fed kidneys, which were suppressed by finerenone (Fig. 3F). Furthermore, transcript levels of collagen-4 alpha chain 2 (Col4a2) and several pro-fibrotic markers including transforming growth factor-β (TGFβ), plasminogen activator inhibitor-1 (Pai1), connective tissue growth factor (CTGF), and tissue inhibitor of metalloproteinase 1 (Timp1) were assessed. Although TGFβ showed

an increasing trend, WD-fed mice exhibited significantly elevated levels of Col4a2, Pai1, CTGF, and Timp1 compared to LF-fed mice. Finerenone treatment lowered these indices to levels observed in LF-fed controls (Fig. 3G). These findings indicate that finerenone significantly attenuates kidney fibrotic remodeling in diet-induced obese mice, underscoring its therapeutic potential in preventing renal injury.

Finerenone decreases kidney triglyceride, cholesterol and ceramides:

Previous studies have established that increased lipid accumulation in the kidney significantly contributes to the pathogenesis of kidney disease in mouse models of diet-induced obesity (59, 61, 62). To evaluate whether finerenone administration influences renal lipid accumulation, we quantified triglyceride and total cholesterol ester levels. Notably, WD-fed mice treated with finerenone showed a significant reduction in renal triglyceride levels. Total kidney cholesterol, which was markedly elevated in WD-fed mice compared to LF-fed controls, was also diminished by finerenone (Fig. 4A). In addition, we extracted lipids and analyzed ceramides by LC-MS. Levels of the long-chain ceramides C24:0 and C26:0 were elevated in kidneys from WD-fed mice compared to LF-fed mice but were significantly reduced following finerenone treatment (Fig. 4B). Our findings demonstrate that finerenone effectively reduces detrimental lipid accumulation in the kidneys of diet-induced obese mice, highlighting its potential to protect against obesity-related kidney damage

Finerenone treatment attenuated the western diet-induced inflammation:

To elucidate the role of inflammation in obesity-induced kidney disease, we examined the infiltration of CD45+ pan-leukocytes and CD68+ macrophages. Mice fed a Western diet (WD) exhibited marked increases in both CD45+ and CD68+ cells compared to low-fat

(LF) controls. However, finerenone administration attenuated the accumulation of these inflammatory cells (Fig. 5A-B). Additionally, WD-fed mice showed a significant upregulation of inflammatory markers (MCP1, NLRP3 inflammasome) and DNA sensor pathways (cGAS, STING). Finerenone treatment reduced the mRNA abundance of these genes to near control levels (Fig. 5C). Consistent with transcript data, Western blot analysis demonstrated elevated STING protein in WD-fed mice, which was suppressed by finerenone. STAT3 is a well-established inflammatory signaling mediator involved in the progression of obesity- and diabetes-related kidney disease (63, 64). Notably, WD feeding led to increased levels of phosphorylated STAT3 (p-STAT3), whereas finerenone significantly reduced p-STAT3 without affecting LF-fed controls (Fig. 5D). Taken together, finerenone inhibits obesity-driven inflammatory cell infiltration and proinflammatory signaling cascades in the kidney, revealing its potential to inhibit inflammation-associated renal damage in diet-induced obesity.

Finerenone ameliorated the mitochondrial morphology and function

Diet-induced obesity leads to mitochondrial dysfunction, characterized by impaired energy metabolism, altered mitochondrial morphology, and reduced oxidative phosphorylation (OXPHOS), all contributing to kidney disease (65-67). To investigate these changes, we used label-free fluorescence lifetime imaging microscopy (FLIM) to measure the ratio of bound to free NADH, thereby estimating the relative rates of glycolysis versus OXPHOS (68-71). A lower free/bound NADH ratio indicates reduced glycolysis and enhanced OXPHOS, while a higher ratio reflects increased glycolysis and diminished OXPHOS. Specifically, we calculated the free-to-bound NADH ratio using the

distinct autofluorescence decay rates of NADH in its free or protein-bound forms. We observed a significant increase in the free/bound NADH ratio in kidney sections from WD-fed mice compared to LF-fed controls. However, this ratio decreased in WD-fed mice receiving finerenone and remained unchanged in LF-fed mice treated with finerenone (Fig. 6A).

Consistent with these findings, electron microscopy revealed that WD-fed mice exhibited profound mitochondrial disorganization, with chaotically distributed and disoriented mitochondria, in contrast to the well-organized mitochondrial arrangement in LF-fed mice. Structural abnormalities in WD-fed mice included cristae fragmentation, homogenization, and swelling of the mitochondrial matrix, along with an increased presence of secondary lysosomes closely associated with damaged mitochondria (yellow arrows) (Fig. 6B, 6C). Finerenone treatment in WD-fed mice effectively improved mitochondrial organization, enhancing both distribution and cristae architecture restoration. In LF-fed mice treated with finerenone, mitochondria remained well-organized and structurally intact, indicating that finerenone had no adverse effects on normal mitochondrial morphology (Fig. 6B). Higher-magnification imaging provided deeper insights into mitochondrial ultrastructure (Fig. 6C). WD-fed mice exhibited severe cristae disorganization, loss of tight packing, and matrix swelling, compared to the densely packed cristae with regular spacing observed in LF-fed mice (Fig. 6C, Panel A and B). In WD-fed mice treated with finerenone, mitochondrial integrity was largely restored, showing more organized cristae, reduced swelling, and overall structural improvement. Morphometric analysis revealed a significant reduction in the number of severely damaged mitochondria, corresponding to Type III and Type IV (Fig. 6C, Panel D; Graphs).

Conversely, finerenone administration had no effect on mitochondrial morphology in LF-fed mice, as their mitochondria remained structurally normal (Fig. 6C, Panel C), nor did it affect the activity of mitochondrial complexes I or IV (Fig. 6D).

Since finerenone enhanced mitochondrial OXPHOS, we next explored possible molecular mechanisms. Previous studies have identified estrogen-related receptors α and γ (ERRα and ERRγ) as critical regulators of mitochondrial OXPHOS and fatty acid oxidation (72, 73). Western blot analysis revealed that the nuclear receptor ERRγ was downregulated in WD-fed mice, with no change in ERRα. Notably, finerenone treatment restored both ERRα and ERRγ expression levels in WD-fed mice but did not alter expression in LF-fed mice (Fig. 6E). Given the recognized role of AMPK in renal cell dysfunction under diet-induced obesity (61), we further examined whether mineralocorticoid receptor inhibition via finerenone activates AMPK signaling. WD-fed mice showed diminished phosphorylated AMPKα (p-AMPKα) relative to total AMPKα, which was significantly restored by finerenone. In contrast, p-AMPKα levels in LF-fed mice were unaffected by finerenone treatment (Fig. 6F). These findings underscore that finerenone effectively counteracts diet-induced mitochondrial dysfunction in the kidneys by enhancing OXPHOS, preserving mitochondrial integrity, and restoring key regulatory pathways (ERR and AMPK), thereby mitigating obesity-related renal damage.

Together, these findings demonstrate that finerenone treatment mitigated WD-induced mitochondrial structural damage and dysfunction.

DISCUSSION

The present study demonstrates that finerenone provides renoprotection in a mouse model of western diet-induced obesity and insulin resistance by modulating mitochondrial homeostasis, inflammation, lipid metabolism and fibrosis. Western diet-fed mice exhibited significant renal dysfunction, marked by increased albuminuria, kidney injury molecule-1 (KIM1), and NGAL and structural abnormalities, including mesangial matrix expansion, podocyte loss, and renal fibrosis, all of which were mitigated by finerenone treatment. Finerenone also reduced pro-inflammatory cytokines, innate immunity pathway activation, and fibrosis markers, lowered kidney cholesterol levels, and restored mitochondrial oxidative phosphorylation. Finerenone uniquely enhanced nuclear receptor ERRγ expression and corrected mitochondrial and ultrastructural abnormalities in WD-fed kidneys. These findings highlight finerenone's multifaceted protective effects on inflammation, fibrosis, and mitochondrial health in WD-induced kidney injury. Finerenone may hold promise as a therapeutic agent for western diet-induced obesity and insulin resistance related kidney damage.

The beneficial effects of finerenone are linked to the upregulation or stabilization of estrogen-related receptor gamma (ERRγ) by modulating mitochondrial biogenesis and oxidative metabolism in renal cells. Enhanced ERRγ signaling improves mitochondrial integrity and function, attenuating lipid accumulation and reducing renal lipotoxicity. Concurrently, these metabolic improvements diminish proinflammatory signaling cascades characterized by reduced levels of proinflammatory cytokines and less infiltration of immune cells thereby diminishing renal inflammation and the progression of kidney injury. MR antagonism effectively prevents glomerular endothelial glycocalyx

(GEnGlx) damage, reduces matrix metalloproteinase (MMP) activity, and restores glomerular albumin permeability in early diabetic nephropathy (DN). that supports MR antagonism as a promising therapeutic strategy to reduce renal damage (58).

In this study, finerenone treatment was initiated after 14 weeks of exposure to a western diet (WD), during which mice develop overt albuminuria as well as kidney and vascular damage. This intervention represents a treatment strategy to assess the efficacy of finerenone in mitigating kidney damage progression in a diet-induced obesity mouse model. Finerenone effectively suppressed the upregulation of key kidney damage markers, including Kim-1, NGAL, TBARS, and albuminuria. Furthermore, it conferred protection against podocyte injury by regulating the actin cytoskeleton protein synaptopodin. Obesity-induced damage to glomerular podocytes has been identified as a primary driver of obesity-related kidney disease (59). High-fat diet (HFD) administration in C57BL/6J mice, prone to diet-induced obesity, increases renal SREBP-1 and SREBP-2 activity and their target enzymes, leading to lipid accumulation, glomerulosclerosis, and proteinuria (59). The protective role of the SGLT2 inhibitor dapagliflozin in reducing kidney and liver complications associated with obesity in western diet-fed mice also supports our findings (62). High fat diet induced kidney disease is marked by the accumulation of lipid vacuoles predominantly in proximal tubular cells, accompanied by impaired mitochondrial morphology, lysosomal dysfunction and disrupted autophagy, suggest that a western diet induces multifaceted renal complications through distinct cellular and metabolic pathways (61, 62). Notably, finerenone not only ameliorated metabolic dysregulation but also prevented diet-induced podocyte injury, further underscoring its renoprotective effects in obesity-associated kidney disease.

The western diet (WD) exacerbates kidney injury, inflammation, and fibrosis through mechanisms that are not entirely attributable to its effects on glucose metabolism. Studies in patients with kidney disease have identified key pro-fibrotic biomarkers, including transforming growth factor-β (TGF-β), monocyte chemoattractant protein-1 (MCP-1), and matrix metalloproteinase-2 (MMP-2), which are strongly associated with fibrosis development and correlate with worsening renal function (74). Preclinical models have been instrumental in elucidating the role of the mineralocorticoid receptor (MR) in the progression of fibrosis and CKD, as well as evaluating the efficacy of finerenone in mitigating renal fibrosis. In the DOCA-salt rat model of CKD, finerenone significantly reduced the renal mRNA expression of the pro-fibrotic marker plasminogen activator inhibitor-1 (PAI-1) and alleviated renal fibrosis, as demonstrated by histopathological analysis (75-77). Additionally, finerenone has been shown to reduce the expression of other critical pro-fibrotic markers, including fibronectin, collagen IV, connective tissue growth factor (CTGF), TGF-β, and MCP-1 (36, 78).

Our findings align with previous studies, reinforcing the evidence that finerenone effectively reduces renal fibrosis and inflammation by targeting multiple pathways associated with these processes (77). The study by Abdeni et al. identified key cell types and gene networks, including secreted posphoprotein 1 (SPP1), interleukin-34 (IL-34), and platelet-derived growth factor subunit b (PDGFb), as drivers of hypertensive nephrosclerosis and fibrosis. It also demonstrated finerenone's superior efficacy in reducing proteinuria and modulating these pathways (79). These findings, validated in human samples, support our study's results, highlighting finerenone's role in kidney protection and its therapeutic potential.

Diet induced obesity significantly contributes to mitochondrial dysfunction, characterized by impaired energy metabolism, altered mitochondrial morphology includes mitochondrial dynamics and reduced oxidative phosphorylation, all of which drive the progression of kidney disease (65-67). Studies in high-fat diet (HFD)-fed mice have shown substantial production of reactive oxygen species (ROS) in the kidneys, accompanied by increased mitochondrial fission, particularly in proximal tubular cells. At the molecular level, the oxidative stress marker Gp91 was markedly upregulated in the kidneys of HFD-fed mice, further highlighting the oxidative stress associated with obesity-induced kidney injury (66). In our study, a notable increase in the free-to-bound NADH ratio was observed in kidney sections from the western diet (WD) fed mice, reflecting increased glycolysis and reduced OXPHOS. This imbalance underscores the metabolic disruptions in mitochondrial energy pathways induced by diet-induced obesity. Importantly, finerenone treatment restored the mitochondrial metabolic balance in the kidneys of WD-fed mice, normalizing the free-to-bound NADH ratio. In addition, we have shown that finenrenone treatment increased complex I activity in western diet fed mcie. These findings suggest that finerenone effectively counteracts the mitochondrial dysfunction caused by diet-induced obesity, potentially restoring renal function.

To uncover the molecular mechanisms underlying the protective effects of finerenone, we investigated nuclear receptors and signaling pathways crucial for mitochondrial regulation. Among these, the estrogen-related receptor γ (ERRγ) is a key regulator of oxidative phosphorylation (OXPHOS) and fatty acid oxidation (80). While ERRγ and its isoform ERRα have been extensively studied in muscle and hepatic cells, their roles in renal mitochondria under metabolic stress remain less understood. Previous research

demonstrated that the PGC-1α/ERRα axis regulates pyruvate dehydrogenase kinase 4 (PDK4) expression, reducing glucose oxidation rates in C2C12 myotubes (81). Additionally, ERRα was found to bind PDK1 and PDK2 in mouse livers, highlighting its role in modulating the metabolic switch between glucose and lipid utilization by mitochondria. Studies have identified estrogen-related receptors (ERRα, ERRβ, and ERRγ) as critical regulators of mitochondrial dysfunction and inflammation in the aging kidney (72). Notably, treatment with a pan-ERR agonist significantly reversed age-related renal damage, including albuminuria, mitochondrial impairment, and inflammation. In alignment with prior research, our study is the first to reveal that a western diet (WD) markedly reduces ERRγ expression in the kidneys, without any significant alterations in ERRα levels (72). Importantly, finerenone treatment restored ERRγ expression in WD-fed animals and increased ERRα expression, further supporting its role in enhancing mitochondrial function. These findings emphasize the critical involvement of ERRs in regulating mitochondrial energy metabolism in renal tissue under conditions of diet-induced obesity.

Given the established role of AMP-activated protein kinase (AMPK) in maintaining mitochondrial homeostasis and its impairment in renal dysfunction associated with obesity (82), we also evaluated AMPK signaling. WD-fed mice exhibited reduced phosphorylated AMPKα (p-AMPKα) levels relative to total AMPKα, indicative of compromised AMPK activity. Notably, finerenone treatment significantly restored p-AMPKα levels, suggesting that mineralocorticoid receptor inhibition reactivates AMPK signaling, promoting mitochondrial function and renal health. Reports have indicated that AMPK activation promotes ERRα expression and facilitates its binding to angiogenic

gene promoters in muscle cells (83). Additionally, suppression of ERRα prevents the AMPK-induced upregulation of angiogenic factors, underscoring the pivotal role of ERRα in this regulatory pathway.

Importantly, obesity significantly contributes to chronic kidney disease (CKD) by promoting comorbid conditions like diabetes and hypertension and causing direct renal damage. This study highlights finerenone's potential as a therapeutic agent, demonstrating its ability to mitigate obesity-induced renal injury through improved mitochondrial function, reduced inflammation, and fibrosis. By restoring key metabolic regulators like ERRγ and AMPK, finerenone preserves renal structure and function. Its efficacy in reducing markers of kidney injury and protecting podocytes underscores its promise in managing obesity-associated CKD. These findings provide a strong rationale for clinical translation to improve outcomes in CKD patients with metabolic dysfunction.

In summary, our findings demonstrate that finerenone mitigates obesity-related renal damage by counteracting mitochondrial dysfunction. It enhances OXPHOS, preserves mitochondrial integrity, and re-establishes key regulatory pathways, including ERRγ and AMPK signaling. These results provide novel mechanistic insights into the renoprotective effects of finerenone and support its therapeutic potential in managing kidney disease associated with diet-induced obesity.

Grants

This work was supported by an Investigator grant from Bayer U.S. LLC, National Institutes of Health (NIH) Grants 2R01DK127830-05 (to M.L.), 1R01DK139676-01A1 (to M.L.).

DISCLOSURES

No conflicts of interest, financial or otherwise, are declared by all the authors.

FIGURE LEGENDS:

Figure 1: Finerenone treatment improved urine parameters in diet-induced obesity. 24-hour urine measured for albumin, kidney injury molecule 1 (KIM1) normalized to creatinine, neutrophil gelatinase-associated lipocalin (NGAL), and thiobarbituric acid reactive substances (TBARS). n=7-9 mice per group, Statistical significance calculated by one-way ANOVA fallowed by Newman-Keuls multiple comparisons test, p-value indicated as $p<0.01$. uACR, albumin creatinine ratio.

Figure 2: Finerenone treatment prevented glomerular histology, ultrastructure, and podocyte function in diet-induced obesity. A) Periodic Acid-Schiff (PAS) staining of kidney sections indicating the accumulation of extracellular matrix proteins within the glomerular mesangial area and positive staining per each glomerulus and considered 20-25 glomeruli per section for quantification. B) Immunofluorescence staining of synaptopodin in the kidney indicates podocyte marker and its relative levels representing the ratio of the synaptopodin positive area within the glomerular tuft area, n=6 per group (A and B). C) SEM images demonstrate the glomerular ultrastructure. Panel A: Normal morphology of the glomerular ultrastructure in LF-fed mice. Panel B: Thickened GBM with disorganized and chaotically distributed PFps. Panel C: Preserved glomerular ultrastructure in LF-fed mice with finerenone. Panel D: Reduced GBM thickness in WD-fed mice following finerenone treatment. Magnifications x 35,000. D) SEM images demonstrate the structure of podocyte foot processes (PFps). In LF-fed mice, PFps show normal distribution and structure, with clearly visible filtration slits and slit diaphragm bridges (arrow). In WD-fed mice, PFps exhibit effacement, widening, degenerative

structural changes, cytoskeletal destruction, foot process fusion, and loss of slit diaphragms. Finerenone treatment in WD-fed mice restores PFps structure and distribution, whith preserved slit diaphragms. The LF+FN group shows normal PFps distribution and slit diaphragms. The bar graphs demonstrate the GBM thickness, PFps number and width. E) TEM images illustrate the glycocalyx distribution in glomerular endothelial cells. In Panel A and C, the glycocalyx appears evenly distributed, exhibits normal density, and covers endothelial pores (arrows) in LF and LF+FN groups. In Panel B, WD-fed mice show a significant reduction in glycocalyx thickness. In Panel D, finerenone treatment in WD mice improves glycocalyx density and distribution. Magnifications x 80,000. F) Enlarged fragments within the highlighted rectangles further illustrate glycocalyx thickness (red line) in mice fed a low-fat (LF), western diet (WD), and those mice treated with finerenone under LF and WD conditions. The bar graph shows quantification of glycocalyx thickness (nm). N=3 per group (C, D, E and F). Data presented as mean ± SEM, with variance analyzed using one-way ANOVA. p-value indicated as $p<0.01$, $p<0.001$.

Figure 3: Finerenone treatment ameliorated Western diet-induced kidney fibrosis. A) Collagen-specific Picrosirius red (PSR) staining highlights collagen deposition in the tubulointerstitial (arrow) and around glomeruli (arrowhead). B) Representative images captured under polarized light microscopy from the same area illustrate collagen distribution. Scale Bar: 50 µm (A and B) C) Quantification of collagen deposition, expressed as a percentage using ImageJ software. Magnification x 20, n = 6 per group. Confocal microscopy images of kidney sections for D) fibronectin expression E) collagen-

IV accumulation, and quantification of the positive staining area considered per each glomerular area performed by Fiji ImageJ software. n=6 per group (A, B, C, D and E). F) qRT-PCR and Immunoblot analysis of fibronectin expression and quantification performed by normalizing to 18srRNA and β-actin (n=4-6 mice per group). G) qRT-PCR analysis of collagen-4 alpha chain2 (Col4a2), plasminogen activator inhibitor (PAI1), transforming growth factor-β (TGFβ), connective tissue growth factor (CTGF) and tissue inhibitor of metalloproteinases-1 (Timp1) and 18srRNA used as the housekeeping gene, n=6 per group. Values are presented as mean ± SEM, with variance calculated using one-way ANOVA with Newman-Keus multiple comparisons test, significance indicated as p-value ($p<0.05$).

Figure 4: Finerenone treatment inhibited renal lipid accumulation in western diet-induced obesity. Total kidney A) triglycerides and cholesterol levels measured by colorimetric assay and bar graphs indicating the quantification, n = 6-8 mice per each group. B) Tissue lipids were extracted, and concentrations were determined by liquid chromatography and mass spectrometry (LC-MS). Graphs indicating the relative levels of long-chain ceramides C24:0 and C26:0, concentrations were quantified using peak-to-peak internal standards and ratios calculated with the tissue weight of individual samples, n = 5-6 per group. Statistical analysis was performed using one-way ANOVA fallowed by Tukey's multiple comparisons test, significance indicated as $p<0.01$ and $p<0.02$.

Figure 5: Finerenone administration reduces the inflammation in the kidneys of western diet-induced obesity. Immunofluorescence staining for A) CD45 as pan leukocyte marker,

B) CD68 as macrophage marker in kidney sections, and percentage of positive staining (indicated as yellow arrow) area quantified, n=6 per group (A and B). C) qRT-PCR showing the gene expression of pro-inflammatory cytokine MCP1 and NLRP3 inflammasome and nucleotide sensors cGAS, sting, and TLR2, n=6 per group. D) Immunoblot analysis indicating the protein expression of sting and phosphorylated stat3 and total stat3. Positive signal density quantified using Fiji Image J, actin used as a control for sting protein, n=4 per group. Statistical analysis was performed using one-way ANOVA with the Newman-Keuls multiple comparisons test, with significance indicated as p values.

Figure 6: Finerenone treatment improved mitochondrial oxidative phosphorylation and morphology. A) Label-free two-photon imaging microscopy was performed to determine the NADH fluorescence lifetime and measured free versus bound NADH ratios indicate the glycolysis versus oxidative phosphorylation (OXPHOS). NADH fluorescence lifetime was quantified using the phasor approach, n=6 per group. B) SEM images illustrate mitochondria in proximal tubule epithelial cells across different groups: low-fat diet (LF, panel A), western diet (WD, panel B), and finerenone treated mice under LF (panel C) and WD (panel D) conditions. Panel A: In LF-fed mice, mitochondria are perpendicularly oriented to the basolateral plasma membrane. Panel B: In WD-fed mice, mitochondria are chaotically distributed and disoriented. Severely damaged mitochondria with condensed cristae (red arrow) are present, along with an increased number of secondary lysosomes closely associated with damaged mitochondria (yellow arrows). Panel C: In LF-fed mice treated with finerenone, mitochondria remain normally distributed. Panel D:

In WD-fed mice, finerenone treatment improves mitochondrial distribution and structure. Magnification: ×35,000. C) Images acquired under higher magnification shows mitochondria ultrastructure in all 4 groups. Panel A: In LF-fed mice, mitochondria appear oval-shaped with longitudinally oriented, regularly spaced, and tightly packed cristae. Panel B: In WD-fed mice, mitochondria exhibit disrupted architecture, with loss of cristae orientation, tightness, and regular spacing. Arrows highlight cristae homogenization and fragmentation within a swollen mitochondrial matrix. Panel C: In LF-fed mice treated with finerenone, mitochondria retain their normal structure. Panel D: In WD-fed mice, finerenone treatment improves mitochondrial structure. Magnification x 50,000. Graphs demonstrate quantification of mitochondrial volume fraction and severity of mitochondrial damage, categorized as follows: Type I: Normal mitochondria with intact structure. Type II: Abnormal mitochondria with irregular shape and size, signs of hypoplasia, swollen cristae, and cristae homogenization in an electron-lucent matrix. Cristae lose longitudinal orientation, tightness, and regular spacing. Type III: Mitochondria with focal disruption of inner membranes, uneven cristae thickening, homogenization, fragmentation, and a swollen electron-lucent matrix. Type IV: Severely damaged mitochondria with outer membrane disruption, cristae loss, and degradation into autophagosomes. Total kidney was homogenized and measured for D) Total complex I and complex IV activity using standard microwell plate assay, n=6-8 per group. Western blot images showing the protein expression of E) nuclear receptors ERRα and ERRγ F) phosphorylated αAMPK and total αAMPK in the kidney and intensity quantified by Fiji Image J, n=4 per group. Statistical analysis was performed using one-way ANOVA with the Newman-Keuls multiple comparisons test, with significance indicated as p values.

REFERENCES:

1. **Kovesdy CP**. Epidemiology of chronic kidney disease: an update 2022. *Kidney Int Suppl (2011)* 12: 7-11, 2022.
2. **Alicic RZ, Rooney MT, and Tuttle KR**. Diabetic Kidney Disease: Challenges, Progress, and Possibilities. *Clin J Am Soc Nephrol* 12: 2032-2045, 2017.
3. **Hoogeveen EK**. The Epidemiology of Diabetic Kidney Disease. *Kidney and Dialysis* 2: 433-442, 2022.
4. **Duru OK, Middleton T, Tewari MK, and Norris K**. The Landscape of Diabetic Kidney Disease in the United States. *Curr Diab Rep* 18: 14, 2018.
5. **Fox CS, Matsushita K, Woodward M, Bilo HJ, Chalmers J, Heerspink HJ, Lee BJ, Perkins RM, Rossing P, Sairenchi T, Tonelli M, Vassalotti JA, Yamagishi K, Coresh J, de Jong PE, Wen CP, Nelson RG, and Chronic Kidney Disease Prognosis C**. Associations of kidney disease measures with mortality and end-stage renal disease in individuals with and without diabetes: a meta-analysis. *Lancet* 380: 1662-1673, 2012.
6. **Stewart S, Kalra PA, Blakeman T, Kontopantelis E, Cranmer-Gordon H, and Sinha S**. Chronic kidney disease: detect, diagnose, disclose-a UK primary care perspective of barriers and enablers to effective kidney care. *BMC Med* 22: 331, 2024.
7. **Yu AS, Pak KJ, Zhou H, Shaw SF, Shi J, Broder BI, and Sim JJ**. All-Cause and Cardiovascular-Related Mortality in CKD Patients With and Without Heart Failure: A Population-Based Cohort Study in Kaiser Permanente Southern California. *Kidney Med* 5: 100624, 2023.
8. **Kounatidis D, Vallianou NG, Stratigou T, Voukali M, Karampela I, and Dalamaga M**. The Kidney in Obesity: Current Evidence, Perspectives and Controversies. *Curr Obes Rep* 13: 680-702, 2024.
9. **Schrauben SJ, Jepson C, Hsu JY, Wilson FP, Zhang X, Lash JP, Robinson BM, Townsend RR, Chen J, Fogelfeld L, Kao P, Landis JR, Rader DJ, Hamm LL, Anderson AH, and Feldman HI**. Insulin resistance and chronic kidney disease progression, cardiovascular events, and death: findings from the chronic renal insufficiency cohort study. *BMC Nephrol* 20: 60, 2019.
10. **Hall ME, do Carmo JM, da Silva AA, Juncos LA, Wang Z, and Hall JE**. Obesity, hypertension, and chronic kidney disease. *Int J Nephrol Renovasc Dis* 7: 75-88, 2014.
11. **Arabi T, Shafqat A, Sabbah BN, Fawzy NA, Shah H, Abdulkader H, Razak A, Sabbah AN, and Arabi Z**. Obesity-related kidney disease: Beyond hypertension and insulin-resistance. *Front Endocrinol (Lausanne)* 13: 1095211, 2022.
12. **Panic A, Stanimirovic J, Sudar-Milovanovic E, and Isenovic ER**. Oxidative stress in obesity and insulin resistance. *Exploration of Medicine* 3: 58-70, 2022.
13. **Fernandez-Sanchez A, Madrigal-Santillan E, Bautista M, Esquivel-Soto J, Morales-Gonzalez A, Esquivel-Chirino C, Durante-Montiel I, Sanchez-Rivera G, Valadez-Vega C, and Morales-Gonzalez JA**. Inflammation, oxidative stress, and obesity. *Int J Mol Sci* 12: 3117-3132, 2011.
14. **Bornstein SR, de Zeeuw D, Heerspink HJL, Schulze F, Cronin L, Wenz A, Tuttle KR, Hadjadj S, and Rossing P**. Aldosterone synthase inhibitor (BI 690517) therapy for people with diabetes and albuminuric chronic kidney disease: A multicentre, randomized, double-blind, placebo-controlled, Phase I trial. *Diabetes Obes Metab* 26: 2128-2138, 2024.
15. **Davis KN, Hines AE, Schaefer MC, and Naseman KW**. Protecting the Kidneys: Update on Therapies to Treat Diabetic Nephropathy. *Clin Diabetes* 40: 305-311, 2022.
16. **Trillini M, and Ruggenenti P**. The risk of CKD progression remains high in patients treated with ACE inhibitors and ARBs, MRAs and SGLT2 inhibitors. Have we already achieved the therapeutic ceiling in CKD? (The CON part). *Clinical Kidney Journal* 17: 2024.
17. **Mann JF, Anderson C, Gao P, Gerstein HC, Boehm M, Ryden L, Sleight P, Teo KK, Yusuf S, and investigators O**. Dual inhibition of the renin-angiotensin system in high-risk

diabetes and risk for stroke and other outcomes: results of the ONTARGET trial. *J Hypertens* 31: 414-421, 2013.
18. **Igarashi M, Hirata A, Kadomoto Y, and Tominaga M**. Dual blockade of angiotensin II with enalapril and losartan reduces proteinuria in hypertensive patients with type 2 diabetes. *Endocr J* 53: 493-501, 2006.
19. **Chen Y, Liu P, Chen X, Li Y, Zhang F, and Wang Y**. Effects of Different Doses of Irbesartan Combined With Spironolactone on Urinary Albumin Excretion Rate in Elderly Patients With Early Type 2 Diabetic Nephropathy. *Am J Med Sci* 355: 418-424, 2018.
20. **Bakris GL, Oparil S, Purkayastha D, Yadao AM, Alessi T, and Sowers JR**. Randomized study of antihypertensive efficacy and safety of combination aliskiren/valsartan vs valsartan monotherapy in hypertensive participants with type 2 diabetes mellitus. *J Clin Hypertens (Greenwich)* 15: 92-100, 2013.
21. **Chiu N, Aggarwal R, Chiu L, Vaduganathan M, Fonarow GC, and Bhatt DL**. Individuals With Chronic Kidney Disease Qualifying for SGLT-2 Inhibitors in the United States and EMPA-KIDNEY Generalizability. *JACC Adv* 2: 100349, 2023.
22. **Chen JJ, Wu CY, Jenq CC, Lee TH, Tsai CY, Tu HT, Huang YT, Yen CL, Yen TH, Chen YC, Tian YC, Yang CW, and Yang HY**. Association of Glucagon-Like Peptide-1 Receptor Agonist vs Dipeptidyl Peptidase-4 Inhibitor Use With Mortality Among Patients With Type 2 Diabetes and Advanced Chronic Kidney Disease. *JAMA Netw Open* 5: e221169, 2022.
23. **Jia G, Lastra G, Bostick BP, LahamKaram N, Laakkonen JP, Yla-Herttuala S, and Whaley-Connell A**. The mineralocorticoid receptor in diabetic kidney disease. *Am J Physiol Renal Physiol* 327: F519-F531, 2024.
24. **Kim DL, Lee SE, and Kim NH**. Renal Protection of Mineralocorticoid Receptor Antagonist, Finerenone, in Diabetic Kidney Disease. *Endocrinol Metab (Seoul)* 38: 43-55, 2023.
25. **Oka T, Sakaguchi Y, Hattori K, Asahina Y, Kajimoto S, Doi Y, Kaimori JY, and Isaka Y**. Mineralocorticoid Receptor Antagonist Use and Hard Renal Outcomes in Real-World Patients With Chronic Kidney Disease. *Hypertension* 79: 679-689, 2022.
26. **Kawanami D, Takashi Y, Muta Y, Oda N, Nagata D, Takahashi H, and Tanabe M**. Mineralocorticoid Receptor Antagonists in Diabetic Kidney Disease. *Front Pharmacol* 12: 754239, 2021.
27. **Agarwal R, Kolkhof P, Bakris G, Bauersachs J, Haller H, Wada T, and Zannad F**. Steroidal and non-steroidal mineralocorticoid receptor antagonists in cardiorenal medicine. *Eur Heart J* 42: 152-161, 2021.
28. **Nguyen Dinh Cat A, Callera GE, Friederich-Persson M, Sanchez A, Dulak-Lis MG, Tsiropoulou S, Montezano AC, He Y, Briones AM, Jaisser F, and Touyz RM**. Vascular dysfunction in obese diabetic db/db mice involves the interplay between aldosterone/mineralocorticoid receptor and Rho kinase signaling. *Sci Rep* 8: 2952, 2018.
29. **Le Billan F, Perrot J, Carceller E, Travers S, Viengchareun S, Kolkhof P, Lombes M, and Fagart J**. Antagonistic effects of finerenone and spironolactone on the aldosterone-regulated transcriptome of human kidney cells. *FASEB J* 35: e21314, 2021.
30. **Tesch GH, and Young MJ**. Mineralocorticoid Receptor Signaling as a Therapeutic Target for Renal and Cardiac Fibrosis. *Front Pharmacol* 8: 313, 2017.
31. **Rossing P, Anker SD, Filippatos G, Pitt B, Ruilope LM, Birkenfeld AL, McGill JB, Rosas SE, Joseph A, Gebel M, Roberts L, Scheerer MF, Bakris GL, Agarwal R, Fidelio DKD, and Investigators F-D**. Finerenone in Patients With Chronic Kidney Disease and Type 2 Diabetes by Sodium-Glucose Cotransporter 2 Inhibitor Treatment: The FIDELITY Analysis. *Diabetes Care* 45: 2991-2998, 2022.
32. **Ghuman JK, and Tuttle KR**. Perspective on Nonsteroidal Mineralocorticoid Receptor Antagonism in Diabetic Kidney Disease. *Kidney360* 3: 744-748, 2022.
33. **Vaduganathan M, Filippatos G, Claggett BL, Desai AS, Jhund PS, Henderson A, Brinker M, Kolkhof P, Schloemer P, Lay-Flurrie J, Viswanathan P, Lam CSP, Senni M, Shah**

SJ, Voors AA, Zannad F, Rossing P, Ruilope LM, Anker SD, Pitt B, Agarwal R, McMurray JJV, and Solomon SD. Finerenone in heart failure and chronic kidney disease with type 2 diabetes: FINE-HEART pooled analysis of cardiovascular, kidney and mortality outcomes. *Nat Med* 30: 3758-3764, 2024.

34. **Nakamura T, Girerd S, Jaisser F, and Barrera-Chimal J**. Nonepithelial mineralocorticoid receptor activation as a determinant of kidney disease. *Kidney Int Suppl (2011)* 12: 12-18, 2022.

35. **Jerome JR, Deliyanti D, Suphapimol V, Kolkhof P, and Wilkinson-Berka JL**. Finerenone, a Non-Steroidal Mineralocorticoid Receptor Antagonist, Reduces Vascular Injury and Increases Regulatory T-Cells: Studies in Rodents with Diabetic and Neovascular Retinopathy. *Int J Mol Sci* 24: 2023.

36. **Droebner K, Pavkovic M, Grundmann M, Hartmann E, Goea L, Nordlohne J, Klar J, Eitner F, and Kolkhof P**. Direct Blood Pressure-Independent Anti-Fibrotic Effects by the Selective Nonsteroidal Mineralocorticoid Receptor Antagonist Finerenone in Progressive Models of Kidney Fibrosis. *Am J Nephrol* 52: 588-601, 2021.

37. **Barrera-Chimal J, Lima-Posada I, Bakris GL, and Jaisser F**. Mineralocorticoid receptor antagonists in diabetic kidney disease - mechanistic and therapeutic effects. *Nat Rev Nephrol* 18: 56-70, 2022.

38. **Abedini A, Sanchez-Navaro A, Wu J, Klotzer KA, Ma Z, Poudel B, Doke T, Balzer MS, Frederick J, Cernecka H, Liu H, Liang X, Vitale S, Kolkhof P, and Susztak K**. Single-cell transcriptomics and chromatin accessibility profiling elucidate the kidney-protective mechanism of mineralocorticoid receptor antagonists. *J Clin Invest* 134: 2024.

39. **Solomon SD, McMurray JJV, Vaduganathan M, Claggett B, Jhund PS, Desai AS, Henderson AD, Lam CSP, Pitt B, Senni M, Shah SJ, Voors AA, Zannad F, Abidin IZ, Alcocer-Gamba MA, Atherton JJ, Bauersachs J, Chang-Sheng M, Chiang CE, Chioncel O, Chopra V, Comin-Colet J, Filippatos G, Fonseca C, Gajos G, Goland S, Goncalvesova E, Kang S, Katova T, Kosiborod MN, Latkovskis G, Lee AP, Linssen GCM, Llamas-Esperon G, Mareev V, Martinez FA, Melenovsky V, Merkely B, Nodari S, Petrie MC, Saldarriaga CI, Saraiva JFK, Sato N, Schou M, Sharma K, Troughton R, Udell JA, Ukkonen H, Vardeny O, Verma S, von Lewinski D, Voronkov L, Yilmaz MB, Zieroth S, Lay-Flurrie J, van Gameren I, Amarante F, Kolkhof P, Viswanathan P, Committees F-H, and Investigators**. Finerenone in Heart Failure with Mildly Reduced or Preserved Ejection Fraction. *N Engl J Med* 391: 1475-1485, 2024.

40. **Guo C, Martinez-Vasquez D, Mendez GP, Toniolo MF, Yao TM, Oestreicher EM, Kikuchi T, Lapointe N, Pojoga L, Williams GH, Ricchiuti V, and Adler GK**. Mineralocorticoid receptor antagonist reduces renal injury in rodent models of types 1 and 2 diabetes mellitus. *Endocrinology* 147: 5363-5373, 2006.

41. **Ferreira JP, Oliveira AC, Vasques-Novoa F, Leite AR, Mendonca L, Zannad F, Butler J, Leite-Moreira A, Saraiva F, and Neves JS**. Mineralocorticoid Receptor Antagonist Combined with SGLT2 Inhibitor versus SGLT2 Inhibitor Alone in Chronic Kidney Disease: A Meta-Analysis of Randomized Trials. *Am J Nephrol* 1-7, 2024.

42. **Kolkhof P, Lawatscheck R, Filippatos G, and Bakris GL**. Nonsteroidal Mineralocorticoid Receptor Antagonism by Finerenone-Translational Aspects and Clinical Perspectives across Multiple Organ Systems. *Int J Mol Sci* 23: 2022.

43. **Gonzalez-Blazquez R, Somoza B, Gil-Ortega M, Martin Ramos M, Ramiro-Cortijo D, Vega-Martin E, Schulz A, Ruilope LM, Kolkhof P, Kreutz R, and Fernandez-Alfonso MS**. Finerenone Attenuates Endothelial Dysfunction and Albuminuria in a Chronic Kidney Disease Model by a Reduction in Oxidative Stress. *Front Pharmacol* 9: 1131, 2018.

44. **Bansal S, Canziani MEF, Birne R, Anker SD, Bakris GL, Filippatos G, Rossing P, Ruilope LM, Farjat AE, Kolkhof P, Lage A, Brinker M, and Pitt B**. Finerenone cardiovascular and kidney outcomes by age and sex: FIDELITY post hoc analysis of two phase 3, multicentre, double-blind trials. *BMJ Open* 14: e076444, 2024.

45. **Zhu Z, Rosenkranz KAT, Kusunoki Y, Li C, Klaus M, Gross O, Angelotti ML, Antonelli G, Cirillo L, Romagnani P, Bouteldja N, Sadr AV, Bulow RD, Boor P, and Anders HJ**. Finerenone Added to RAS/SGLT2 Blockade for CKD in Alport Syndrome. Results of a Randomized Controlled Trial with Col4a3-/- Mice. *J Am Soc Nephrol* 34: 1513-1520, 2023.
46. **Marzolla V, Feraco A, Gorini S, Mammi C, Marrese C, Mularoni V, Boitani C, Lombes M, Kolkhof P, Ciriolo MR, Armani A, and Caprio M**. The novel non-steroidal MR antagonist finerenone improves metabolic parameters in high-fat diet-fed mice and activates brown adipose tissue via AMPK-ATGL pathway. *FASEB J* 34: 12450-12465, 2020.
47. **Odermatt A**. The Western-style diet: a major risk factor for impaired kidney function and chronic kidney disease. *Am J Physiol Renal Physiol* 301: F919-931, 2011.
48. **Hariharan D, Vellanki K, and Kramer H**. The Western Diet and Chronic Kidney Disease. *Curr Hypertens Rep* 17: 16, 2015.
49. **Kil HN, Eom SY, Park JD, Kawamoto T, Kim YD, and Kim H**. A rapid method for estimating the levels of urinary thiobarbituric Acid reactive substances for environmental epidemiologic survey. *Toxicol Res* 30: 7-11, 2014.
50. **Fraga CG, Leibovitz BE, and Tappel AL**. Lipid peroxidation measured as thiobarbituric acid-reactive substances in tissue slices: characterization and comparison with homogenates and microsomes. *Free Radic Biol Med* 4: 155-161, 1988.
51. **Myakala K, Jones BA, Wang XX, and Levi M**. Sacubitril/valsartan treatment has differential effects in modulating diabetic kidney disease in db/db mice and KKAy mice compared with valsartan treatment. *Am J Physiol Renal Physiol* 320: F1133-F1151, 2021.
52. **Myakala K, Wang XX, Shults NV, Krawczyk E, Jones BA, Yang X, Rosenberg AZ, Ginley B, Sarder P, Brodsky L, Jang Y, Na CH, Qi Y, Zhang X, Guha U, Wu C, Bansal S, Ma J, Cheema A, Albanese C, Hirschey MD, Yoshida T, Kopp JB, Panov J, and Levi M**. NAD metabolism modulates inflammation and mitochondria function in diabetic kidney disease. *J Biol Chem* 299: 104975, 2023.
53. **Thibodeau JF, Holterman CE, Burger D, Read NC, Reudelhuber TL, and Kennedy CR**. A novel mouse model of advanced diabetic kidney disease. *PLoS One* 9: e113459, 2014.
54. **Weibel ER, Kistler GS, and Scherle WF**. Practical stereological methods for morphometric cytology. *J Cell Biol* 30: 23-38, 1966.
55. **Costanzo V, and Costanzo M**. Intravital Imaging with Two-Photon Microscopy: A Look into the Kidney. *Photonics* 9: 294, 2022.
56. **Han SJ, Jang HS, Noh MR, Kim J, Kong MJ, Kim JI, Park JW, and Park KM**. Mitochondrial NADP(+)-Dependent Isocitrate Dehydrogenase Deficiency Exacerbates Mitochondrial and Cell Damage after Kidney Ischemia-Reperfusion Injury. *J Am Soc Nephrol* 28: 1200-1215, 2017.
57. **Stasi A, Cosola C, Caggiano G, Cimmarusti MT, Palieri R, Acquaviva PM, Rana G, and Gesualdo L**. Obesity-Related Chronic Kidney Disease: Principal Mechanisms and New Approaches in Nutritional Management. *Front Nutr* 9: 925619, 2022.
58. **Crompton M, Ferguson JK, Ramnath RD, Onions KL, Ogier AS, Gamez M, Down CJ, Skinner L, Wong KH, Dixon LK, Sutak J, Harper SJ, Pontrelli P, Gesualdo L, Heerspink HL, Toto RD, Welsh GI, Foster RR, Satchell SC, and Butler MJ**. Mineralocorticoid receptor antagonism in diabetes reduces albuminuria by preserving the glomerular endothelial glycocalyx. *JCI Insight* 8: 2023.
59. **Jiang T, Wang Z, Proctor G, Moskowitz S, Liebman SE, Rogers T, Lucia MS, Li J, and Levi M**. Diet-induced obesity in C57BL/6J mice causes increased renal lipid accumulation and glomerulosclerosis via a sterol regulatory element-binding protein-1c-dependent pathway. *J Biol Chem* 280: 32317-32325, 2005.
60. **van der Heijden RA, Bijzet J, Meijers WC, Yakala GK, Kleemann R, Nguyen TQ, de Boer RA, Schalkwijk CG, Hazenberg BP, Tietge UJ, and Heeringa P**. Obesity-induced chronic

inflammation in high fat diet challenged C57BL/6J mice is associated with acceleration of age-dependent renal amyloidosis. *Sci Rep* 5: 16474, 2015.
61. **Decleves AE, Zolkipli Z, Satriano J, Wang L, Nakayama T, Rogac M, Le TP, Nortier JL, Farquhar MG, Naviaux RK, and Sharma K**. Regulation of lipid accumulation by AMP-activated kinase [corrected] in high fat diet-induced kidney injury. *Kidney Int* 85: 611-623, 2014.
62. **Wang D, Luo Y, Wang X, Orlicky DJ, Myakala K, Yang P, and Levi M**. The Sodium-Glucose Cotransporter 2 Inhibitor Dapagliflozin Prevents Renal and Liver Disease in Western Diet Induced Obesity Mice. *Int J Mol Sci* 19: 2018.
63. **Yu JT, Fan S, Li XY, Hou R, Hu XW, Wang JN, Shan RR, Dong ZH, Xie MM, Dong YH, Shen XY, Jin J, Wen JG, Liu MM, Wang W, and Meng XM**. Novel insights into STAT3 in renal diseases. *Biomed Pharmacother* 165: 115166, 2023.
64. **Pace J, Paladugu P, Das B, He JC, and Mallipattu SK**. Targeting STAT3 signaling in kidney disease. *Am J Physiol Renal Physiol* 316: F1151-F1161, 2019.
65. **Andres-Hernando A, Lanaspa MA, Kuwabara M, Orlicky DJ, Cicerchi C, Bales E, Garcia GE, Roncal-Jimenez CA, Sato Y, and Johnson RJ**. Obesity causes renal mitochondrial dysfunction and energy imbalance and accelerates chronic kidney disease in mice. *Am J Physiol Renal Physiol* 317: F941-F948, 2019.
66. **Sun Y, Ge X, Li X, He J, Wei X, Du J, Sun J, Li X, Xun Z, Liu W, Zhang H, Wang ZY, and Li YC**. High-fat diet promotes renal injury by inducing oxidative stress and mitochondrial dysfunction. *Cell Death Dis* 11: 914, 2020.
67. **Zheng P, Ma W, Gu Y, Wu H, Bian Z, Liu N, Yang D, and Chen X**. High-fat diet causes mitochondrial damage and downregulation of mitofusin-2 and optic atrophy-1 in multiple organs. *J Clin Biochem Nutr* 73: 61-76, 2023.
68. **Datta R, Heylman C, George SC, and Gratton E**. Label-free imaging of metabolism and oxidative stress in human induced pluripotent stem cell-derived cardiomyocytes. *Biomed Opt Express* 7: 1690-1701, 2016.
69. **Stringari C, Cinquin A, Cinquin O, Digman MA, Donovan PJ, and Gratton E**. Phasor approach to fluorescence lifetime microscopy distinguishes different metabolic states of germ cells in a live tissue. *Proc Natl Acad Sci U S A* 108: 13582-13587, 2011.
70. **Ranjit S, Henriksen K, Dvornikov A, Delsante M, Rosenberg A, Levi M, and Gratton E**. Phasor approach to autofluorescence lifetime imaging FLIM can be a quantitative biomarker of chronic renal parenchymal injury. *Kidney Int* 98: 1341-1346, 2020.
71. **Ranjit S, Lanzano L, Libby AE, Gratton E, and Levi M**. Advances in fluorescence microscopy techniques to study kidney function. *Nat Rev Nephrol* 17: 128-144, 2021.
72. **Wang XX, Myakala K, Libby AE, Krawczyk E, Panov J, Jones BA, Bhasin K, Shults N, Qi Y, Krausz KW, Zerfas PM, Takahashi S, Daneshpajouhnejad P, Titievsky A, Taranenko E, Billon C, Chatterjee A, Elgendy B, Walker JK, Albanese C, Kopp JB, Rosenberg AZ, Gonzalez FJ, Guha U, Brodsky L, Burris TP, and Levi M**. Estrogen-Related Receptor Agonism Reverses Mitochondrial Dysfunction and Inflammation in the Aging Kidney. *Am J Pathol* 193: 1969-1987, 2023.
73. **Dhillon P, Park J, Hurtado Del Pozo C, Li L, Doke T, Huang S, Zhao J, Kang HM, Shrestra R, Balzer MS, Chatterjee S, Prado P, Han SY, Liu H, Sheng X, Dierickx P, Batmanov K, Romero JP, Prosper F, Li M, Pei L, Kim J, Montserrat N, and Susztak K**. The Nuclear Receptor ESRRA Protects from Kidney Disease by Coupling Metabolism and Differentiation. *Cell Metab* 33: 379-394 e378, 2021.
74. **Meng XM, Nikolic-Paterson DJ, and Lan HY**. Inflammatory processes in renal fibrosis. *Nat Rev Nephrol* 10: 493-503, 2014.
75. **Kolkhof P, Lawatscheck R, Filippatos G, and Bakris GL**. Nonsteroidal Mineralocorticoid Receptor Antagonism by Finerenone—Translational Aspects and Clinical Perspectives across Multiple Organ Systems. *International Journal of Molecular Sciences* 23: 9243, 2022.

76. **Kolkhof P, Delbeck M, Kretschmer A, Steinke W, Hartmann E, Bärfacker L, Eitner F, Albrecht-Küpper B, and Schäfer S**. Finerenone, a Novel Selective Nonsteroidal Mineralocorticoid Receptor Antagonist Protects From Rat Cardiorenal Injury. *Journal of Cardiovascular Pharmacology* 64: 69-78, 2014.
77. **Chen W, Zheng L, Wang J, Lin Y, and Zhou T**. Overview of the safety, efficiency, and potential mechanisms of finerenone for diabetic kidney diseases. *Front Endocrinol (Lausanne)* 14: 1320603, 2023.
78. **Di Lullo L, Lavalle C, Scatena A, Mariani MV, Ronco C, and Bellasi A**. Finerenone: Questions and Answers-The Four Fundamental Arguments on the New-Born Promising Non-Steroidal Mineralocorticoid Receptor Antagonist. *J Clin Med* 12: 2023.
79. **Abedini A, Zhu YO, Chatterjee S, Halasz G, Devalaraja-Narashimha K, Shrestha R, M SB, Park J, Zhou T, Ma Z, Sullivan KM, Hu H, Sheng X, Liu H, Wei Y, Boustany-Kari CM, Patel U, Almaani S, Palmer M, Townsend R, Blady S, Hogan J, Morton L, Susztak K, and Investigators TS**. Urinary Single-Cell Profiling Captures the Cellular Diversity of the Kidney. *J Am Soc Nephrol* 32: 614-627, 2021.
80. **Zhao J, Lupino K, Wilkins BJ, Qiu C, Liu J, Omura Y, Allred AL, McDonald C, Susztak K, Barish GD, and Pei L**. Genomic integration of ERRgamma-HNF1beta regulates renal bioenergetics and prevents chronic kidney disease. *Proc Natl Acad Sci U S A* 115: E4910-E4919, 2018.
81. **Wende AR, Huss JM, Schaeffer PJ, Giguere V, and Kelly DP**. PGC-1alpha coactivates PDK4 gene expression via the orphan nuclear receptor ERRalpha: a mechanism for transcriptional control of muscle glucose metabolism. *Mol Cell Biol* 25: 10684-10694, 2005.
82. **Juszczak F, Caron N, Mathew AV, and Decleves AE**. Critical Role for AMPK in Metabolic Disease-Induced Chronic Kidney Disease. *Int J Mol Sci* 21: 2020.
83. **Sopariwala DH, Rios AS, Park MK, Song MS, Kumar A, and Narkar VA**. Estrogen-related receptor alpha is an AMPK-regulated factor that promotes ischemic muscle revascularization and recovery in diet-induced obese mice. *FASEB Bioadv* 4: 602-618, 2022.

Table 1

	LF	LF + finerenone	WD	WD + finerenone
Body weight (g)	35.16 ± 1.4	36.86 ± 1.69	47.15 ± 1.4*	45.74 ± 1.41
Kidney weight (g)/body weight ratis (KW/BW)	0.01 ± 0.0007	0.009 ± 0.0003	0.009 ± 0.001	0.008 ± 0.0003#
Blood glucose	177.9 ± 0.6	178.5 ± 0.6	177.6 ± 1.25	176.4 ± 0.6
Plasma Triglycerides (mg/dL)	95.58 ± 12.08	107.7 ± 15.4	163 ± 15.8*	147.2 ± 15.4
Plasma Cholesterol (mg/dL)	183.3 ± 2.1	181.2 ± 2.1	308.8 ± 68.16*	240.7 ± 68.16#
Systolic blood pressure (mmHg)	109.6 ± 3.16	112.7 ± 1.9	112.8 ± 3.72	109 ± 2.97

Statistical significance calculated as one-way ANOVA with Newman-Keuls multiple comparision, values presented as means ± SEM (N=8 per group), * vs LF group, # vs WD group

Figure 1

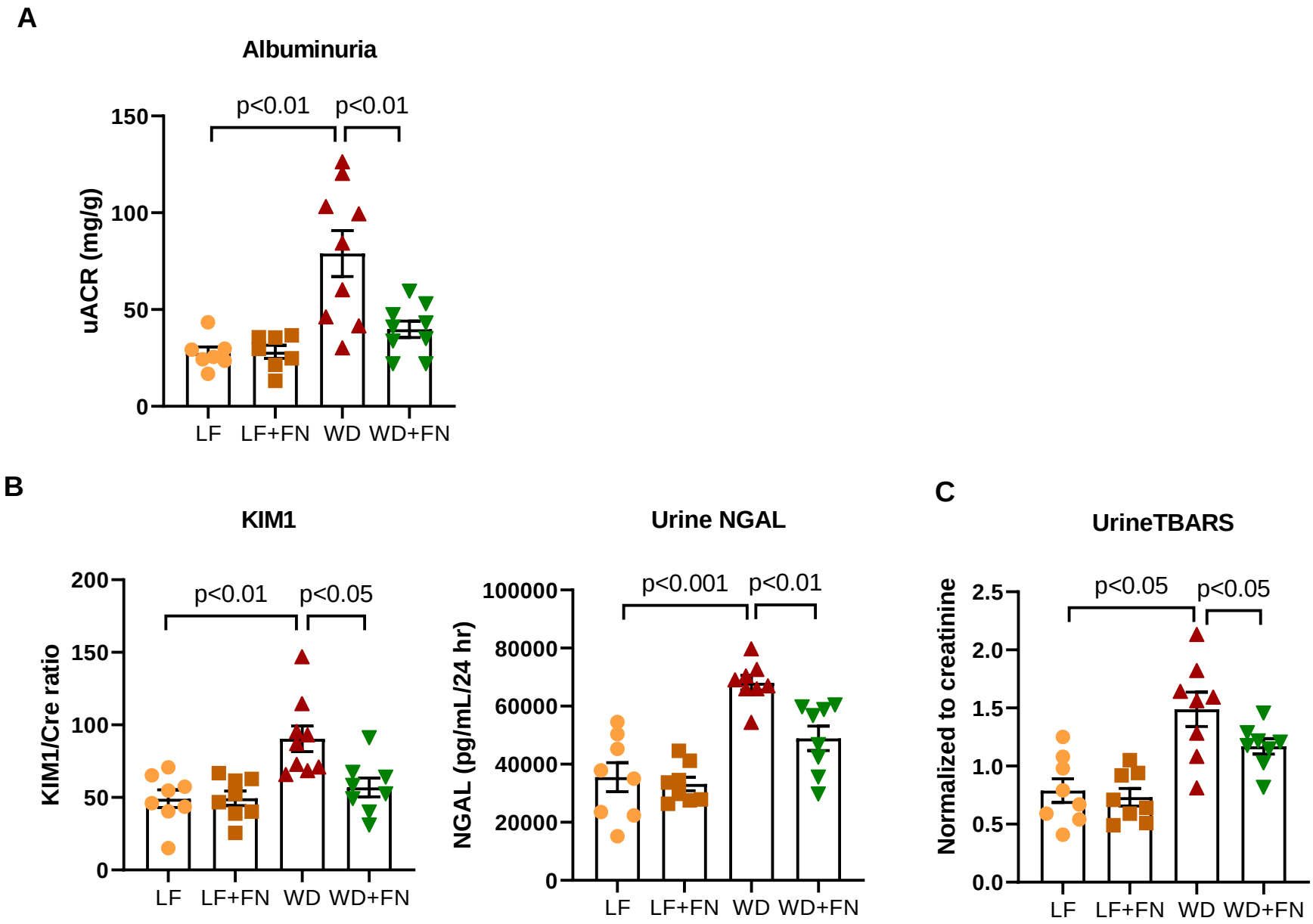
A
Albuminuria
p<0.01
p<0.01
uACR (mg/g)
150
100
50
0
LF
LF+FN
WD
WD+FN
B
KIM1
p<0.01
p<0.05
KIM1/Cre ratio
200
150
100
50
0
LF
LF+FN
WD
WD+FN
Urine NGAL
p<0.001
p<0.01
NGAL (pg/mL/24 hr)
100000
80000
60000
40000
20000
0
LF
LF+FN
WD
WD+FN
C
UrineTBARS
p<0.05
p<0.05
Normalized to creatinine
2.5
2.0
1.5
1.0
0.5
0.0
LF
LF+FN
WD
WD+FN

Figure 2

A

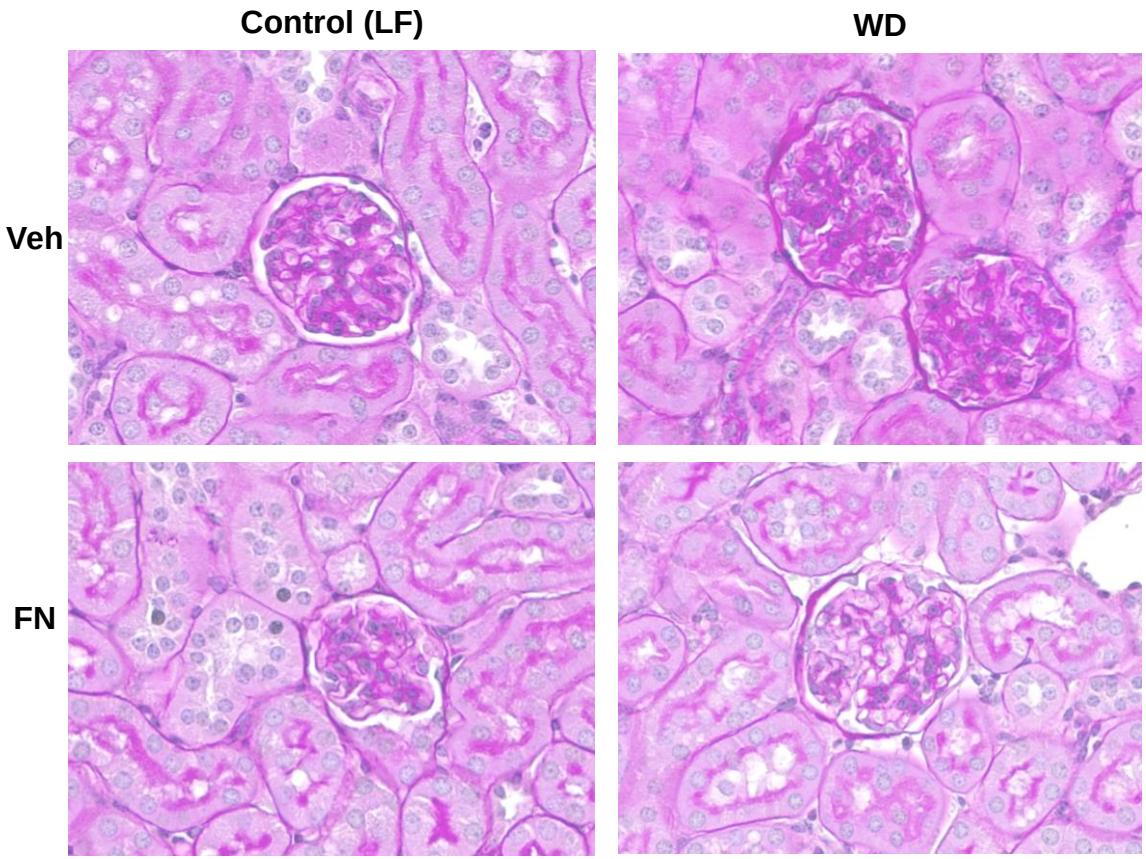
Control (LF)
WD
Veh
FN

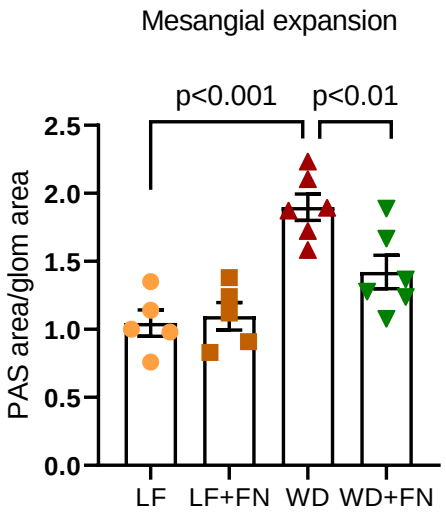
Mesangial expansion
p<0.001
p<0.01
PAS area/glom area
2.5
2.0
1.5
1.0
0.5
0.0
LF
LF+FN
WD
WD+FN

Figure 2

B

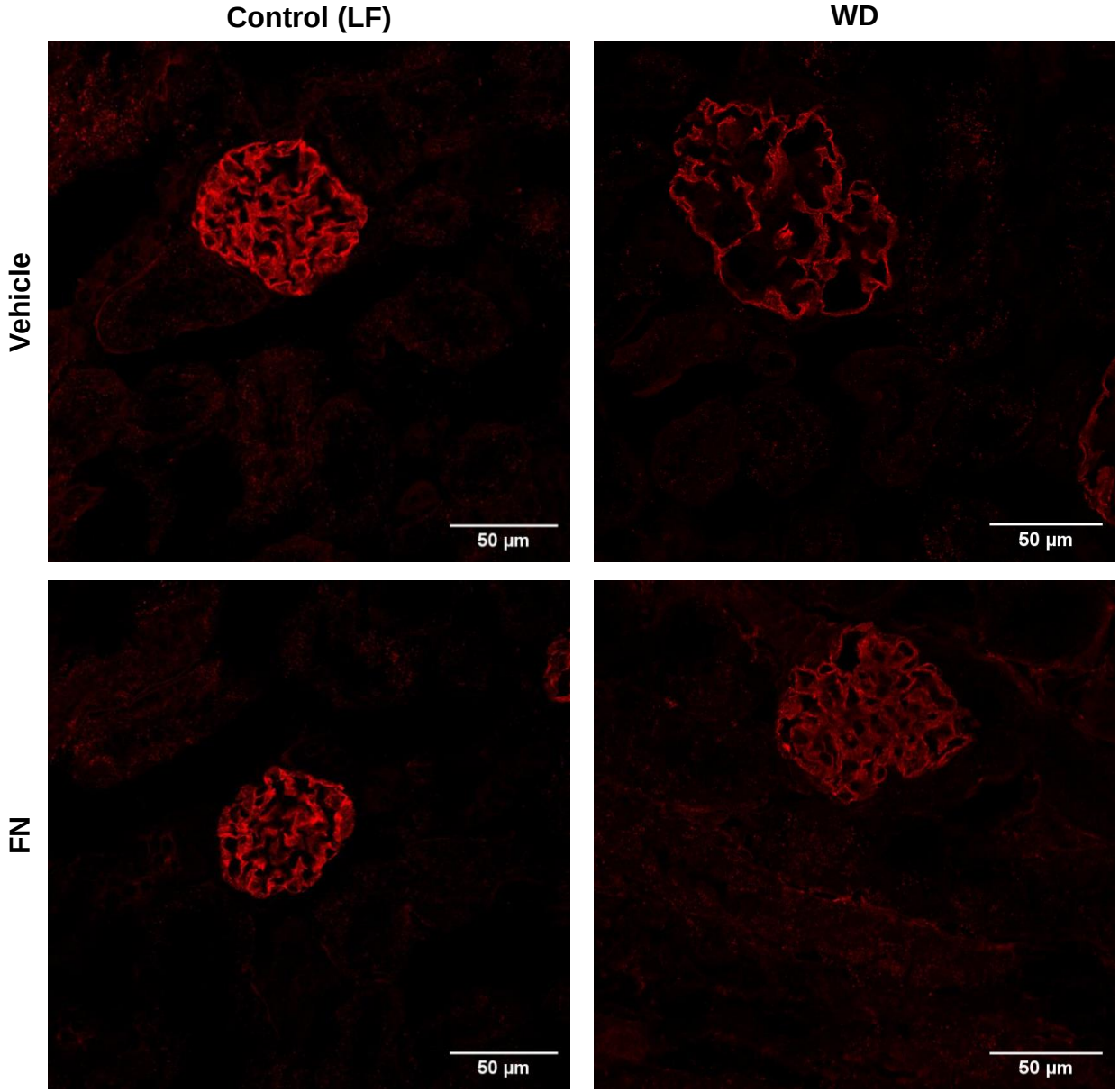
Control (LF)
WD
Vehicle
FN
50 µm
50 µm
50 µm
50 µm

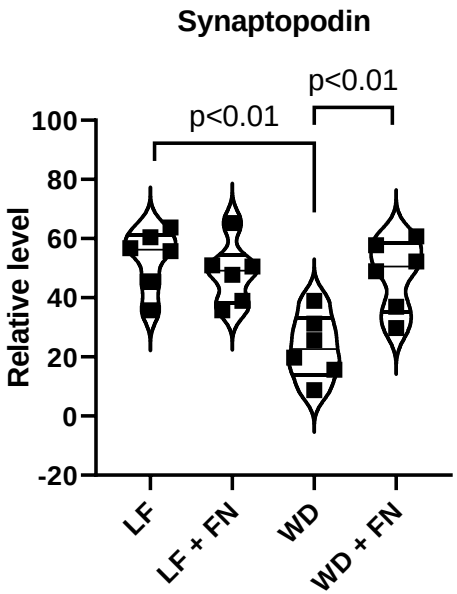
Synaptopodin
p<0.01
p<0.01
Relative level
100
80
60
40
20
0
-20
LF
LF + FN
WD
WD + FN

Figure 2

C

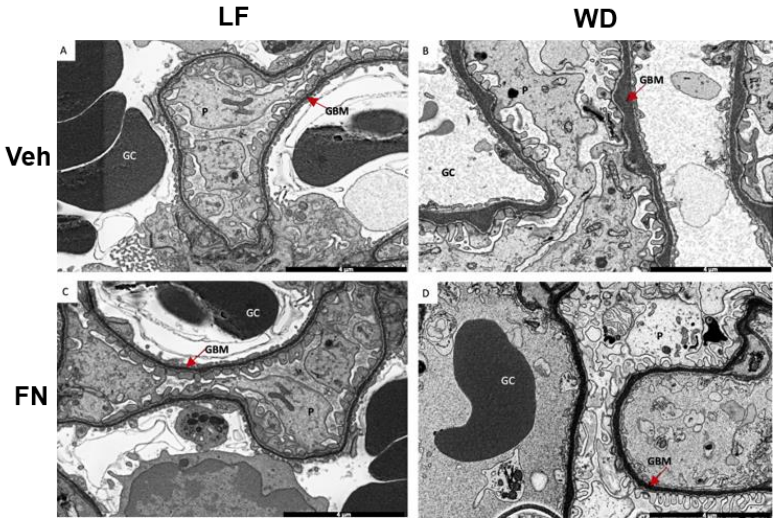
LF
WD
Veh
FN
A
B
C
D
GBM
GC
P

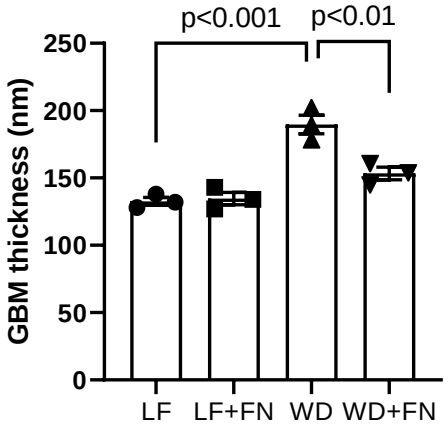
p<0.001
p<0.01
GBM thickness (nm)
250
200
150
100
50
0
LF
LF+FN
WD
WD+FN

D

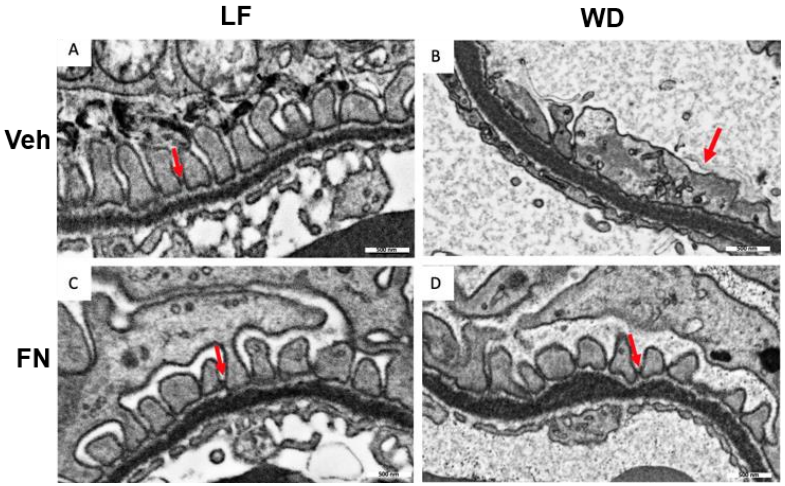
LF
WD
Veh
FN
A
B
C
D

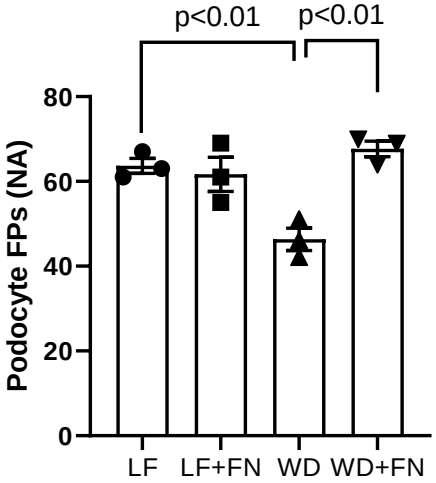
p<0.01
p<0.01
Podocyte FPs (NA)
80
60
40
20
0
LF
LF+FN
WD
WD+FN

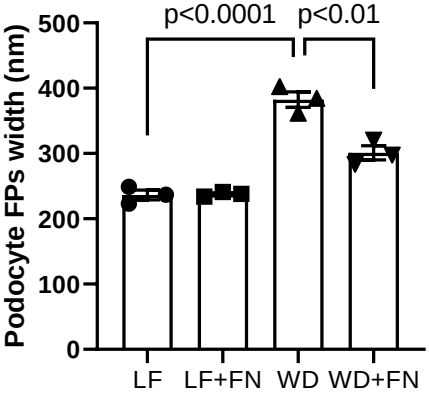
p<0.0001
p<0.01
Podocyte FPs width (nm)
500
400
300
200
100
0
LF
LF+FN
WD
WD+FN

Figure 2

E

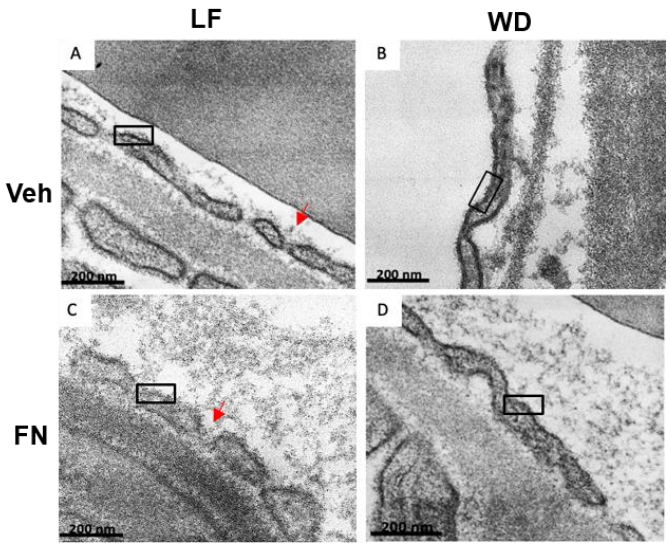
LF
WD
Veh
FN
A
B
C
D
200 nm

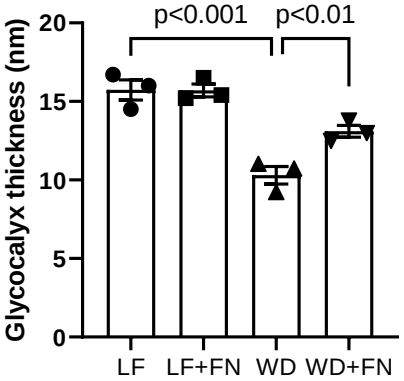
p<0.001
p<0.01
Glycocalyx thickness (nm)
20
15
10
5
0
LF
LF+FN
WD
WD+FN

F

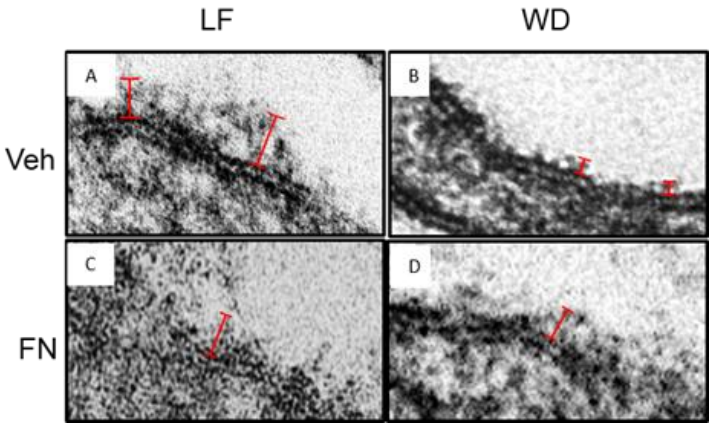
LF
WD
Veh
FN
A
B
C
D

Figure 3

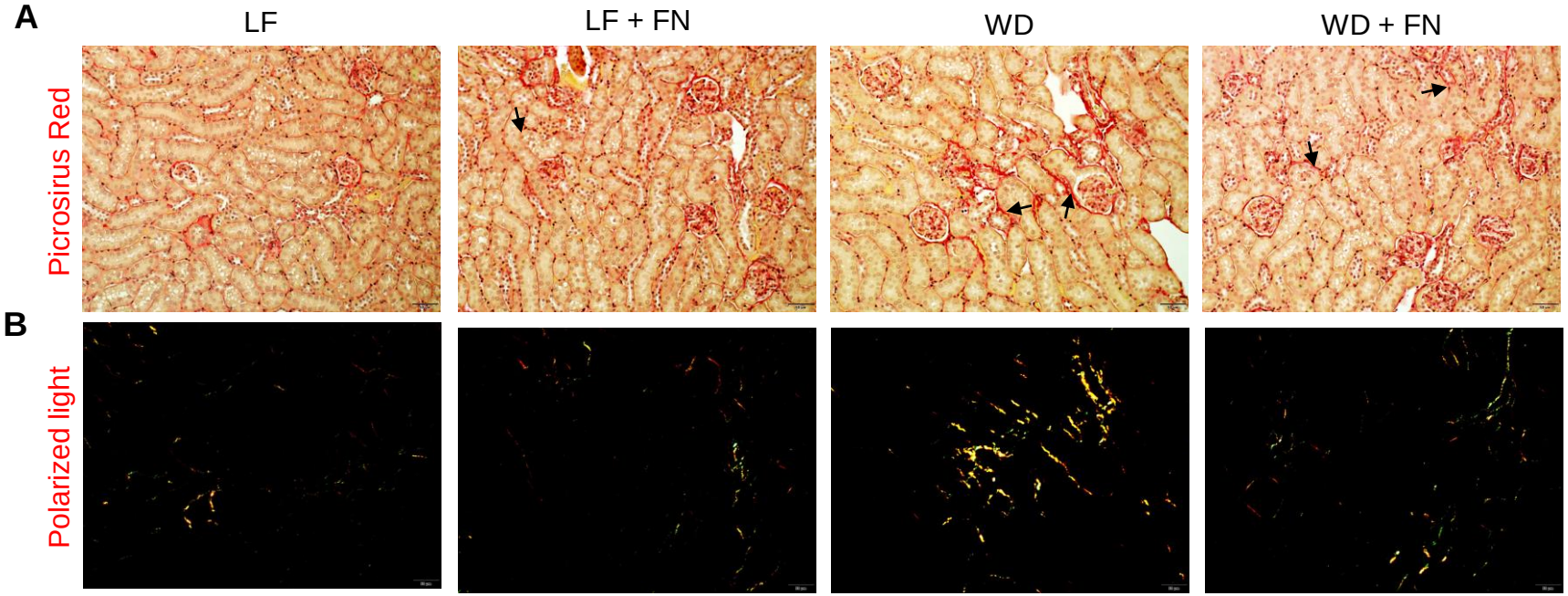
A
LF
LF + FN
WD
WD + FN
Picrosirus Red
B
Polarized light

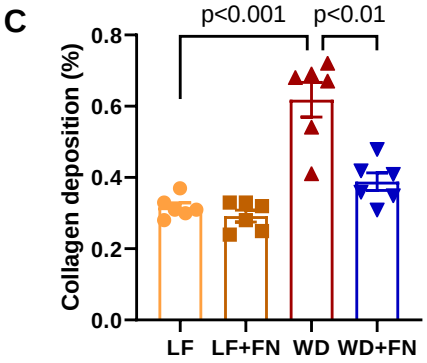
C
p<0.001
p<0.01
Collagen deposition (%)
0.8
0.6
0.4
0.2
0.0
LF
LF+FN
WD
WD+FN

Figure 3

D

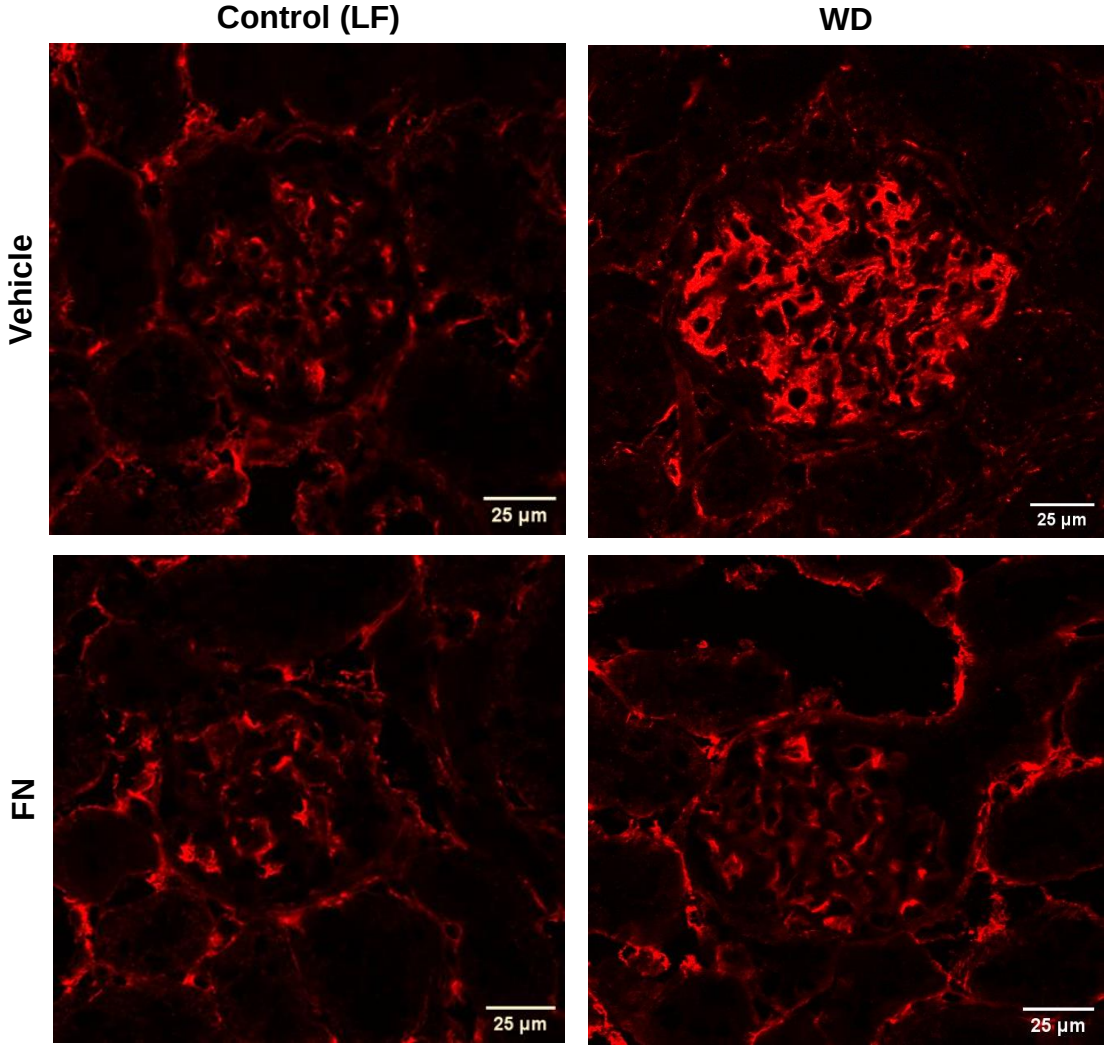
Control (LF)
WD
Vehicle
FN
25 µm
25 µm
25 µm
25 µm

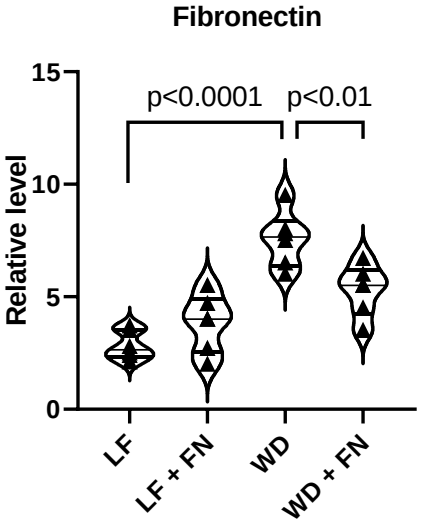
Fibronectin
Relative level
15
10
5
0
p<0.0001
p<0.01
LF
LF + FN
WD
WD + FN

Figure 3

E

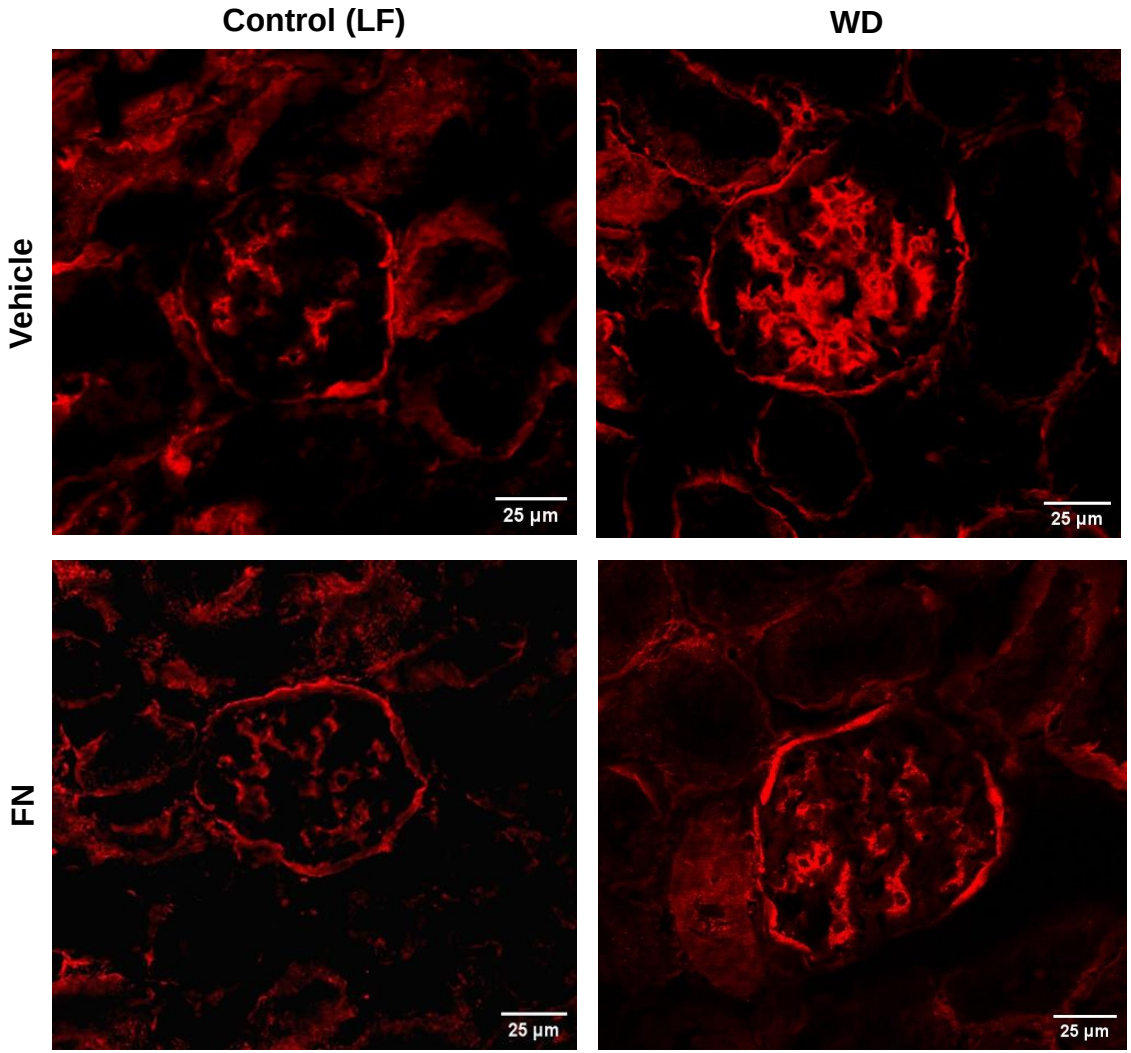
Control (LF)
WD
Vehicle
FN
25 µm
25 µm
25 µm
25 µm

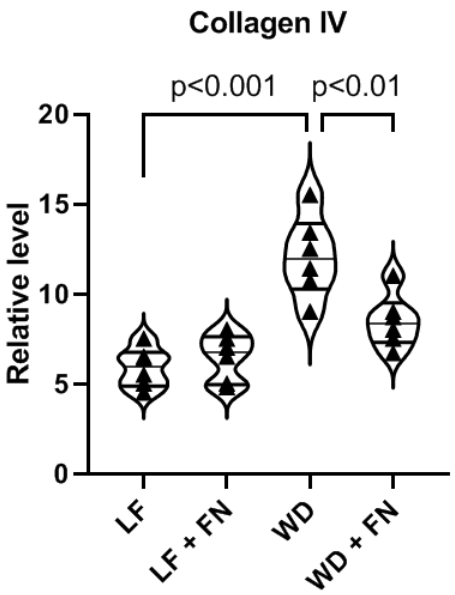
Collagen IV
p<0.001
p<0.01
Relative level
20
15
10
5
0
LF
LF + FN
WD
WD + FN

Figure 3

F

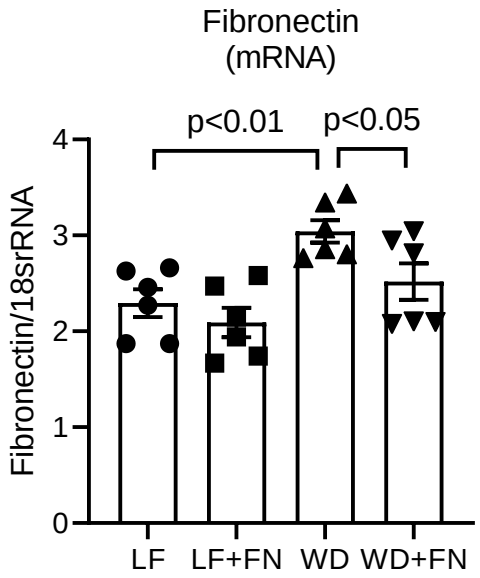
Fibronectin
(mRNA)
p<0.01
p<0.05
Fibronectin/18srRNA
4
3
2
1
0
LF
LF+FN
WD
WD+FN

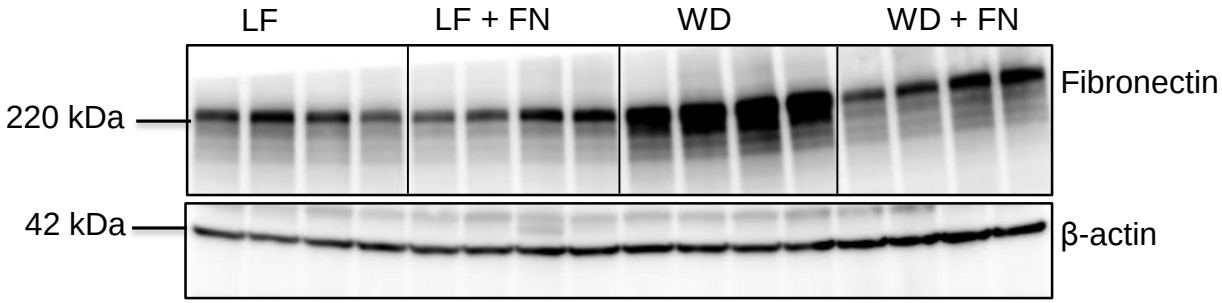
LF
LF + FN
WD
WD + FN
220 kDa
42 kDa
Fibronectin
β-actin

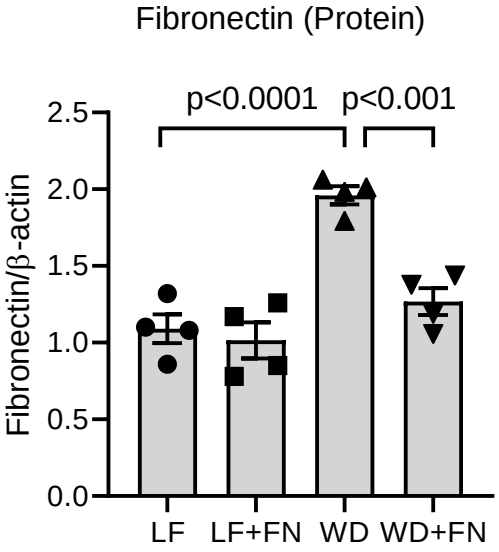
Fibronectin (Protein)
p<0.0001
p<0.001
Fibronectin/β-actin
2.5
2.0
1.5
1.0
0.5
0.0
LF
LF+FN
WD
WD+FN

Figure 3

G

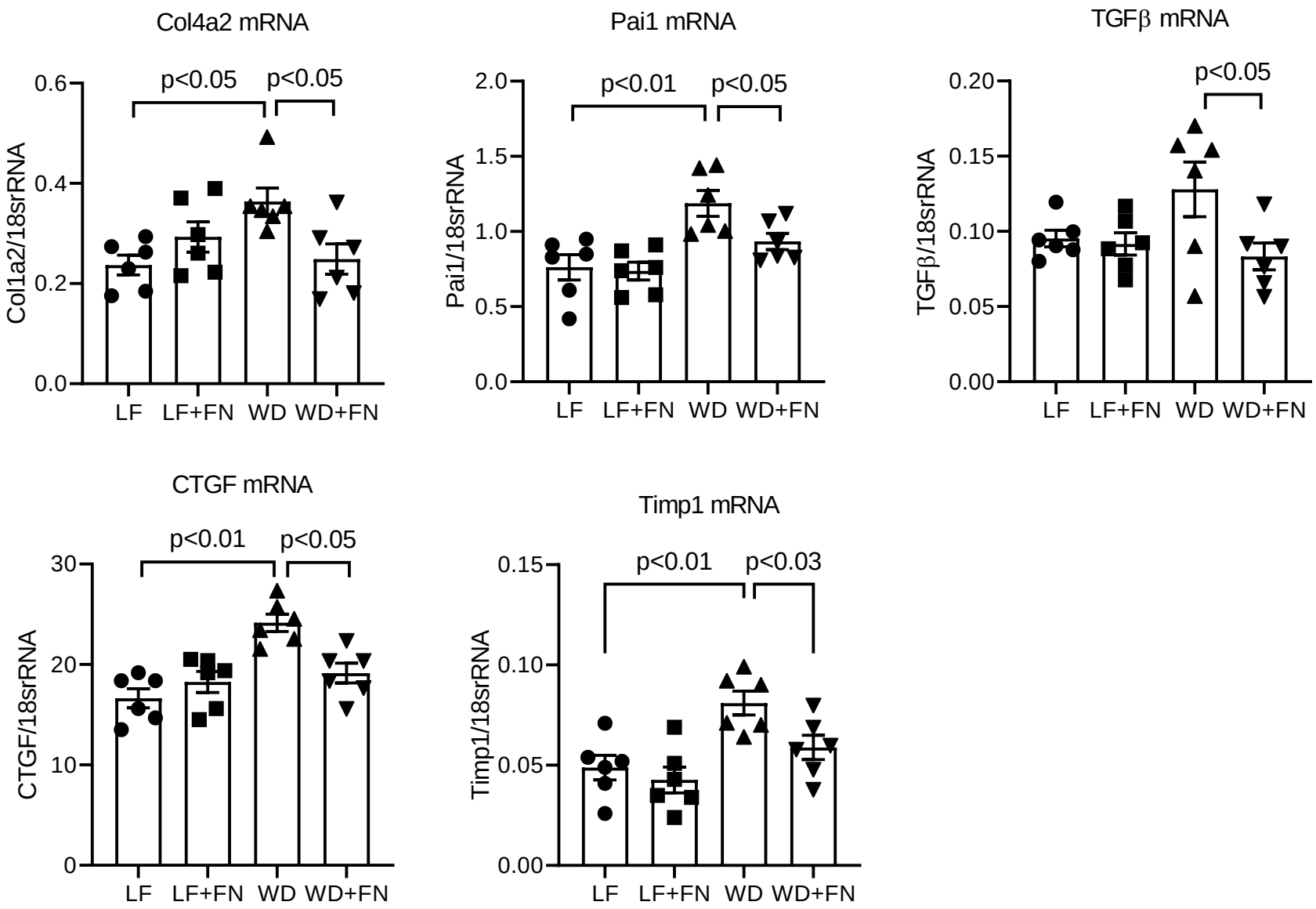
Col4a2 mRNA
Col1a2/18srRNA
0.6
0.4
0.2
0.0
p<0.05
p<0.05
LF
LF+FN
WD
WD+FN
Pai1 mRNA
Pai1/18srRNA
2.0
1.5
1.0
0.5
0.0
p<0.01
p<0.05
LF
LF+FN
WD
WD+FN
TGFβ mRNA
TGFβ/18srRNA
0.20
0.15
0.10
0.05
0.00
p<0.05
LF
LF+FN
WD
WD+FN
CTGF mRNA
CTGF/18srRNA
30
20
10
0
p<0.01
p<0.05
LF
LF+FN
WD
WD+FN
Timp1 mRNA
Timp1/18srRNA
0.15
0.10
0.05
0.00
p<0.01
p<0.03
LF
LF+FN
WD
WD+FN

Figure 4

A

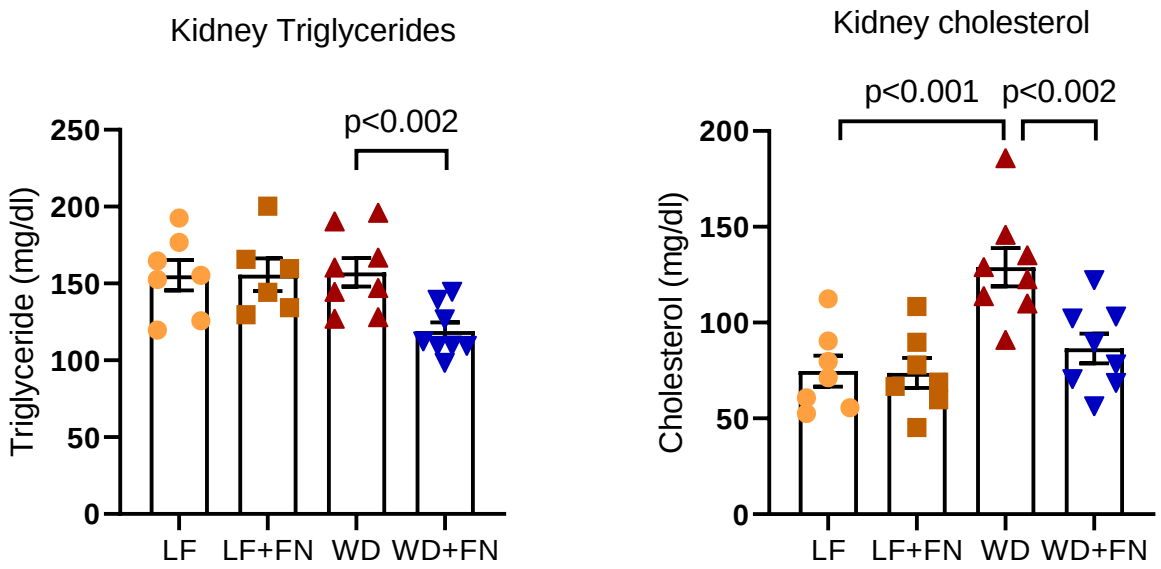
Kidney Triglycerides
p<0.002
Triglyceride (mg/dl)
250
200
150
100
50
0
LF
LF+FN
WD
WD+FN
Kidney cholesterol
p<0.001
p<0.002
Cholesterol (mg/dl)
200
150
100
50
0
LF
LF+FN
WD
WD+FN

B

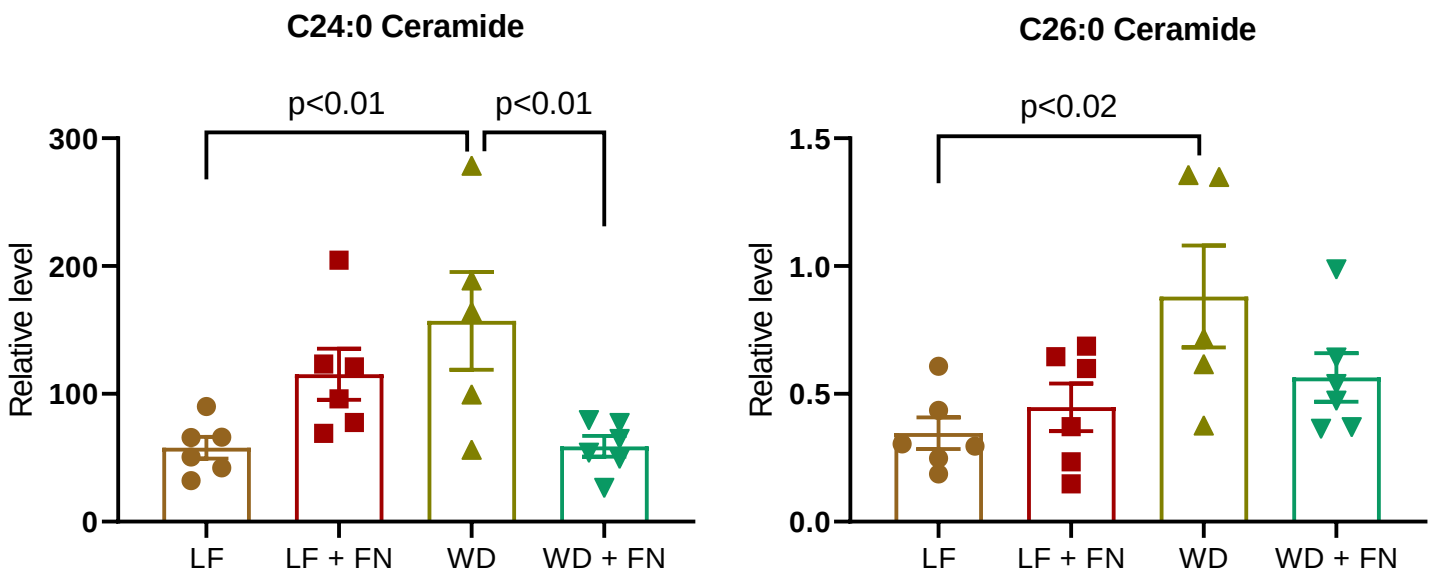
C24:0 Ceramide
p<0.01
p<0.01
Relative level
300
200
100
0
LF
LF + FN
WD
WD + FN
C26:0 Ceramide
p<0.02
Relative level
1.5
1.0
0.5
0.0
LF
LF + FN
WD
WD + FN

Figure 5

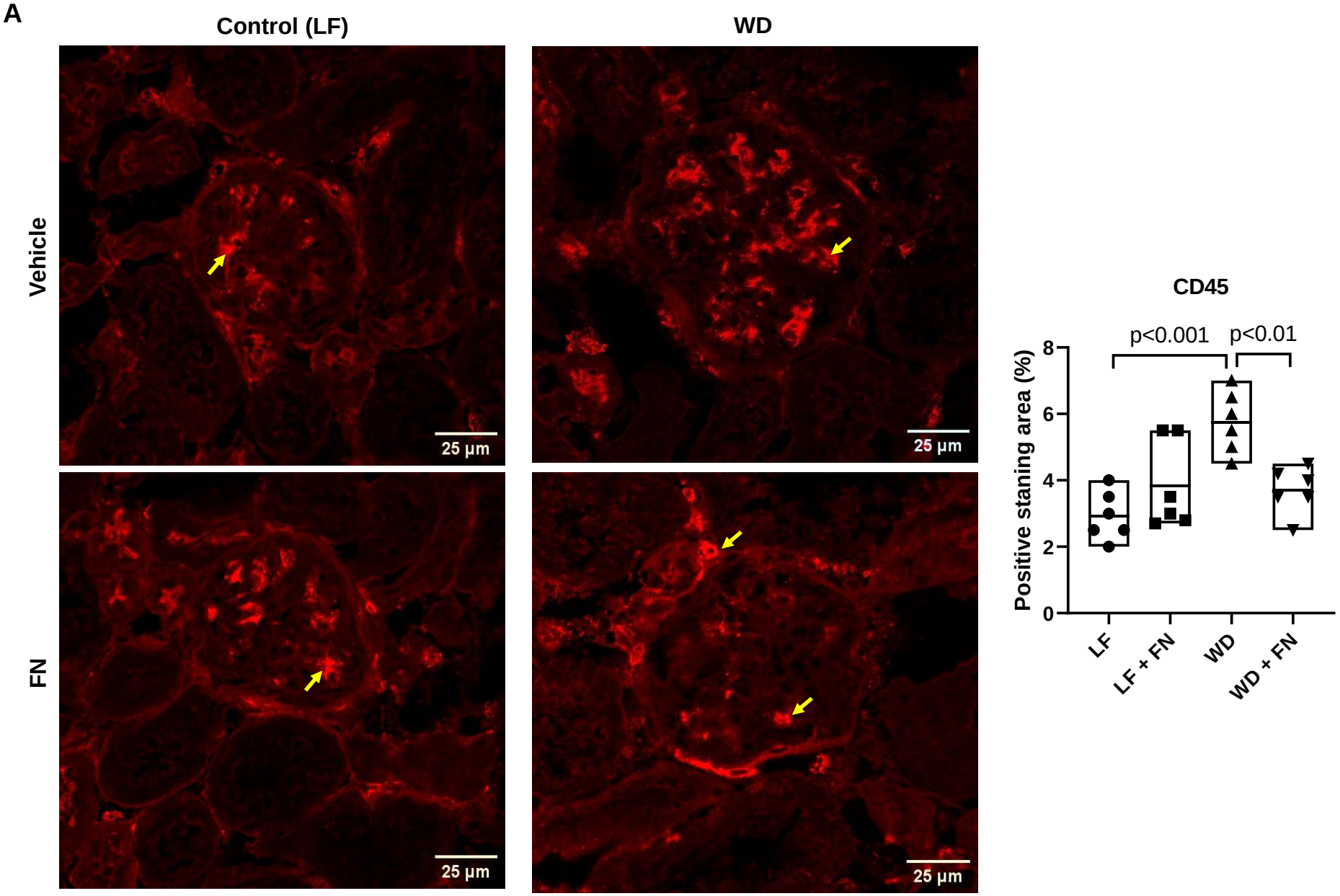
A
Control (LF)
WD
Vehicle
FN
25 µm
25 µm
25 µm
25 µm
CD45
p<0.001
p<0.01
Positive staning area (%)
0
2
4
6
8
LF
LF + FN
WD
WD + FN

Figure 5

B

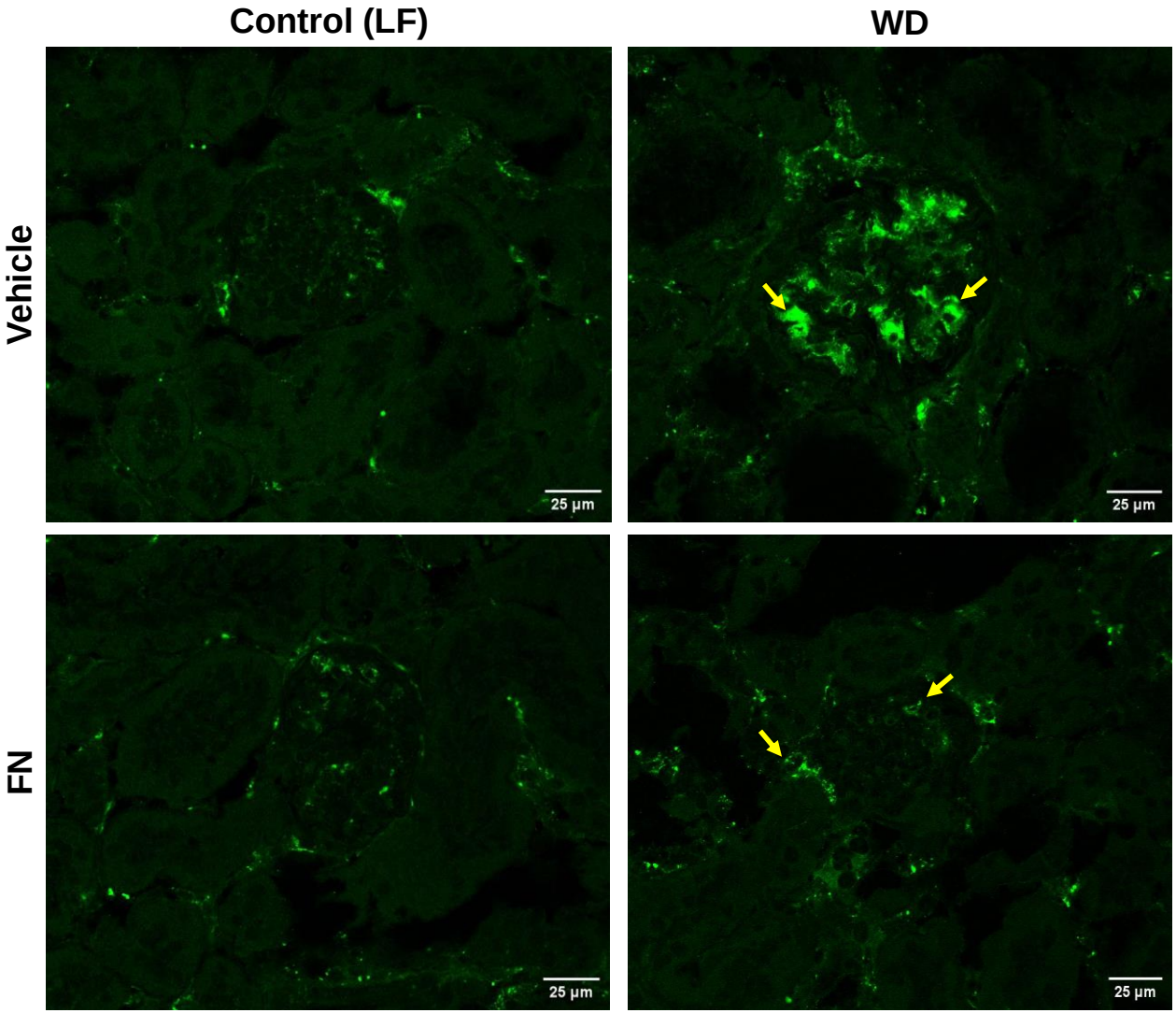
Control (LF)
WD
Vehicle
FN
25 µm
25 µm
25 µm
25 µm

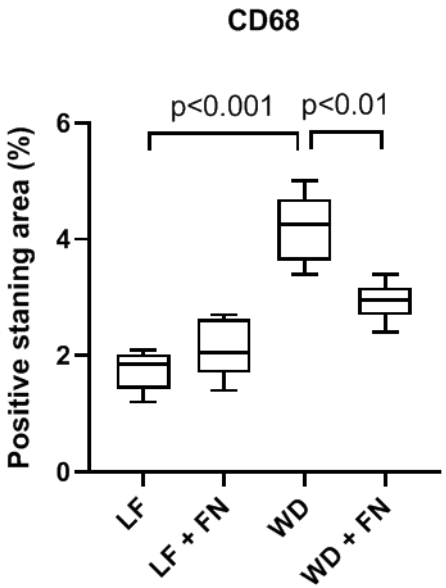
CD68
p<0.001
p<0.01
Positive staning area (%)
0
2
4
6
LF
LF + FN
WD
WD + FN

Figure 5

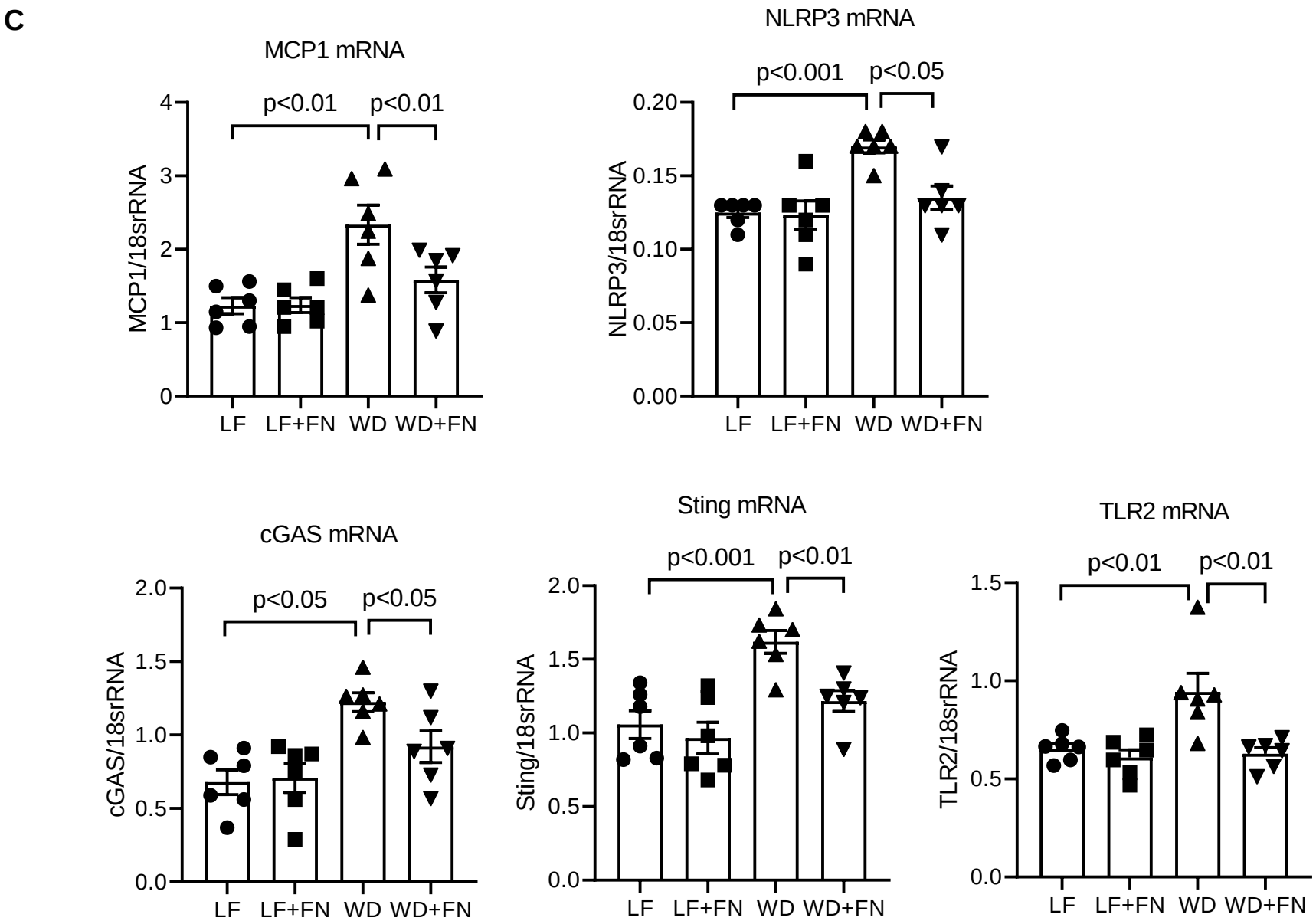
c
MCP1 mRNA
p<0.01
p<0.01
MCP1/18srRNA
0
1
2
3
4
LF
LF+FN
WD
WD+FN
NLRP3 mRNA
p<0.001
p<0.05
NLRP3/18srRNA
0.00
0.05
0.10
0.15
0.20
LF
LF+FN
WD
WD+FN
cGAS mRNA
p<0.05
p<0.05
cGAS/18srRNA
0.0
0.5
1.0
1.5
2.0
LF
LF+FN
WD
WD+FN
Sting mRNA
p<0.001
p<0.01
Sting/18srRNA
0.0
0.5
1.0
1.5
2.0
LF
LF+FN
WD
WD+FN
TLR2 mRNA
p<0.01
p<0.01
TLR2/18srRNA
0.0
0.5
1.0
1.5
LF
LF+FN
WD
WD+FN

Figure 5

D

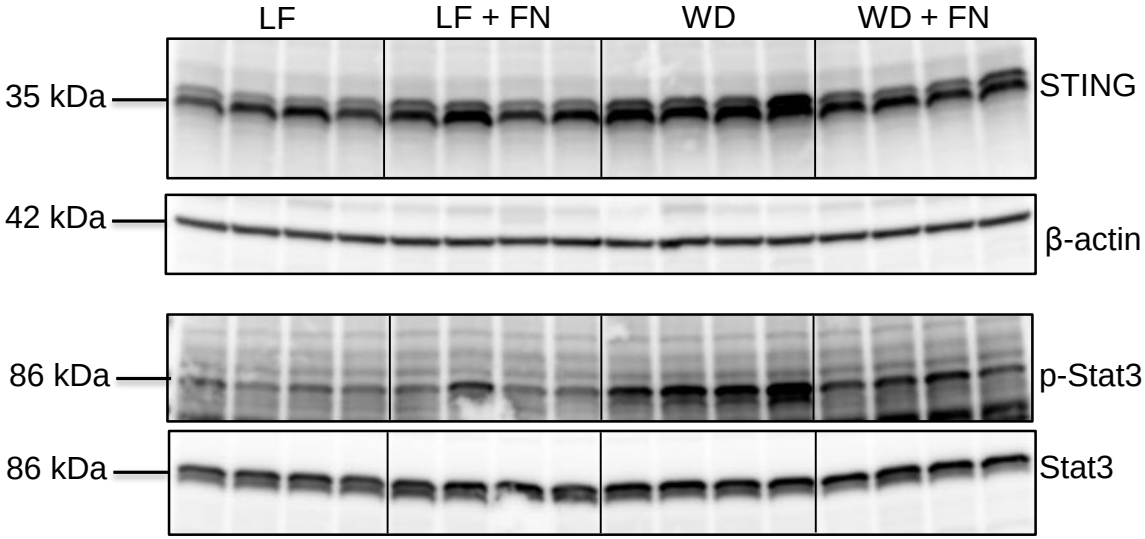
LF
LF + FN
WD
WD + FN
35 kDa
STING
42 kDa
β-actin
86 kDa
p-Stat3
86 kDa
Stat3

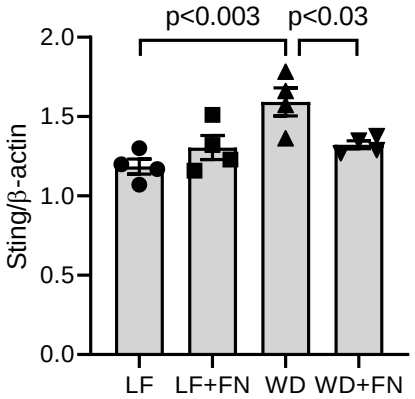
p<0.003
p<0.03
Sting/β-actin
2.0
1.5
1.0
0.5
0.0
LF
LF+FN
WD
WD+FN

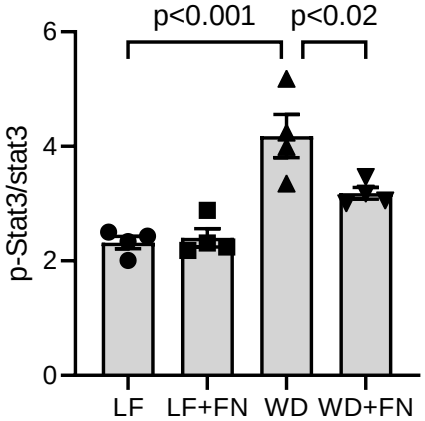
p<0.001
p<0.02
p-Stat3/stat3
6
4
2
0
LF
LF+FN
WD
WD+FN

Figure 6

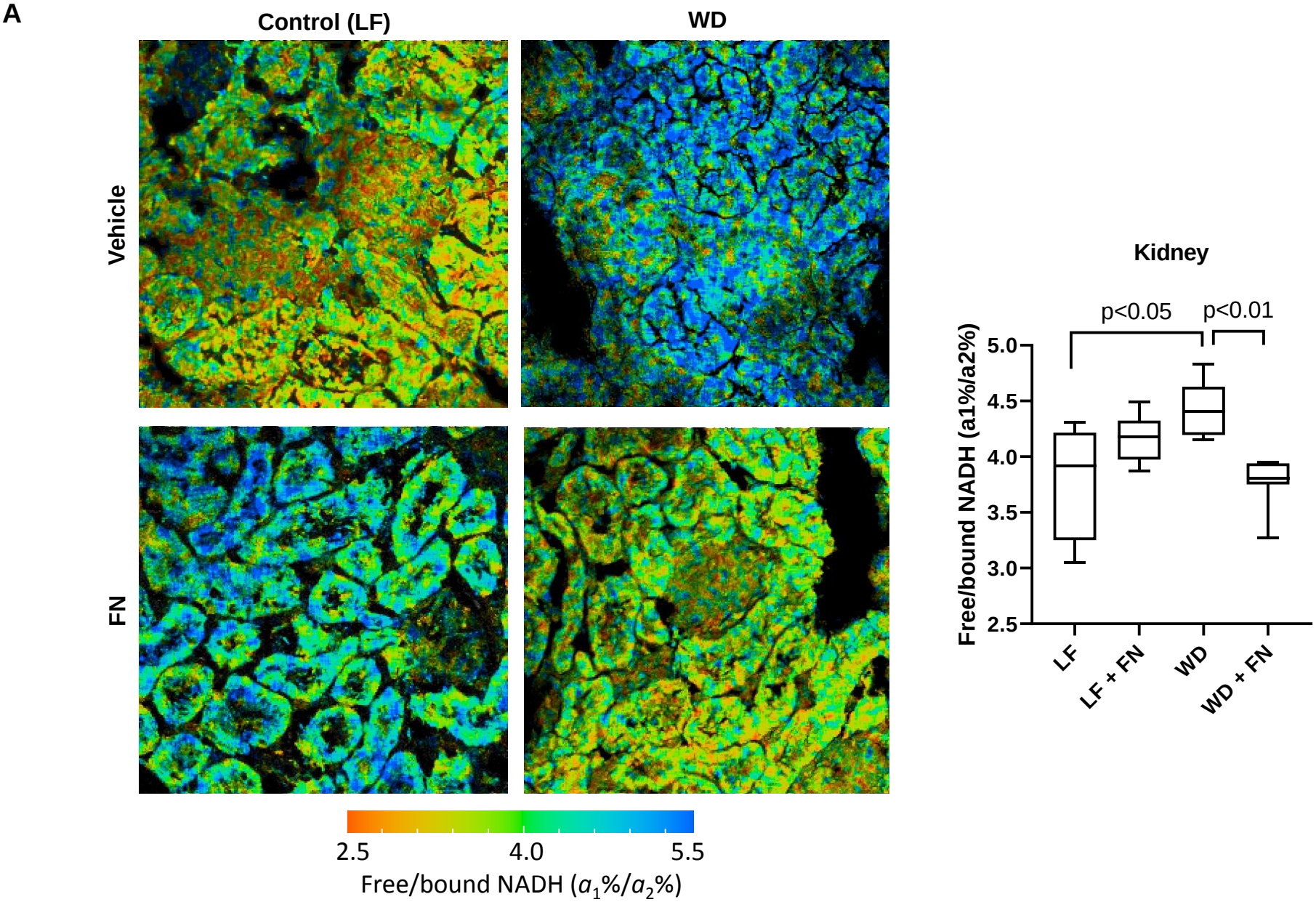
A
Control (LF)
WD
Vehicle
FN
2.5
4.0
5.5
Free/bound NADH (a_1%/a_2%)
Kidney
p<0.05
p<0.01
Free/bound NADH (a1%/a2%)
5.0
4.5
4.0
3.5
3.0
2.5
LF
LF + FN
WD
WD + FN

Figure 6

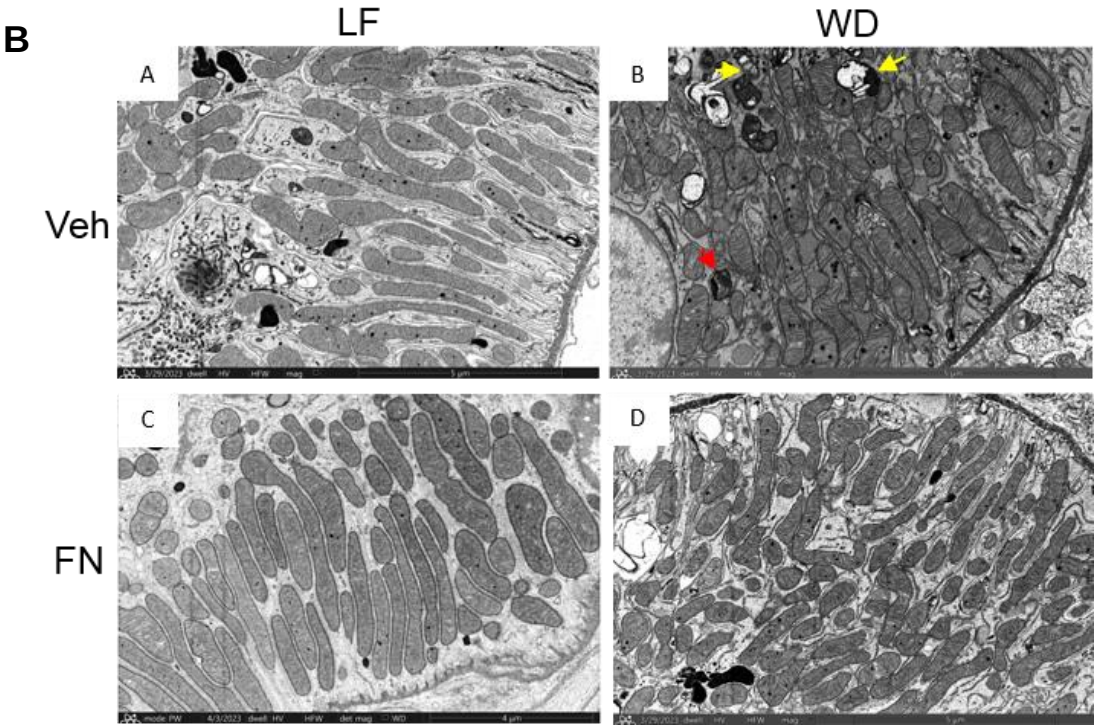
B
LF
WD
A
B
Veh
C
D
FN

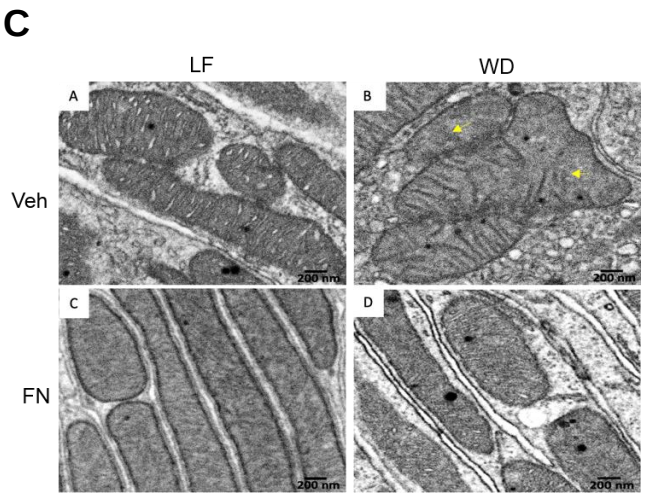
C
LF
WD
A
B
Veh
C
D
FN
200 nm

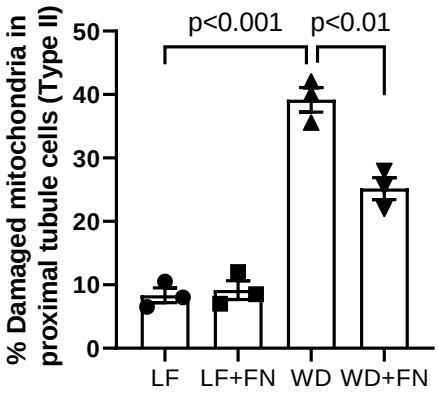
% Damaged mitochondria in proximal tubule cells (Type II)
p<0.001
p<0.01
50
40
30
20
10
0
LF
LF+FN
WD
WD+FN

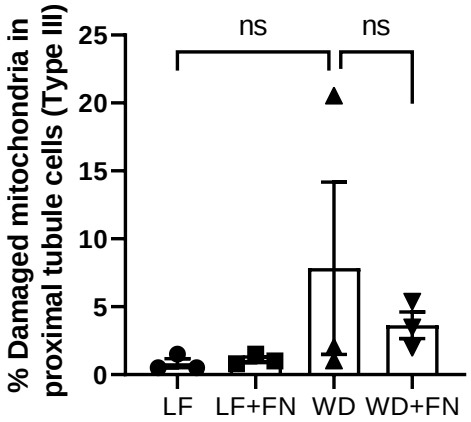
% Damaged mitochondria in proximal tubule cells (Type III)
ns
ns
25
20
15
10
5
0
LF
LF+FN
WD
WD+FN

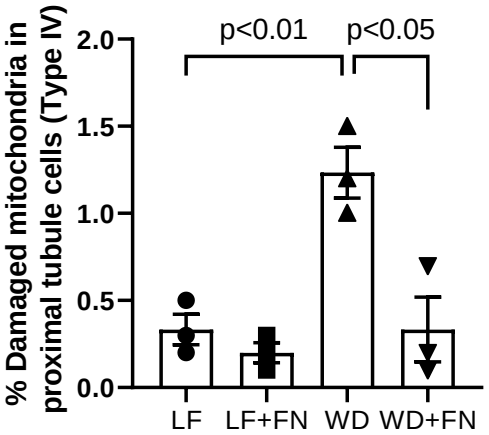
% Damaged mitochondria in proximal tubule cells (Type IV)
p<0.01
p<0.05
2.0
1.5
1.0
0.5
0.0
LF
LF+FN
WD
WD+FN

Figure 6

D

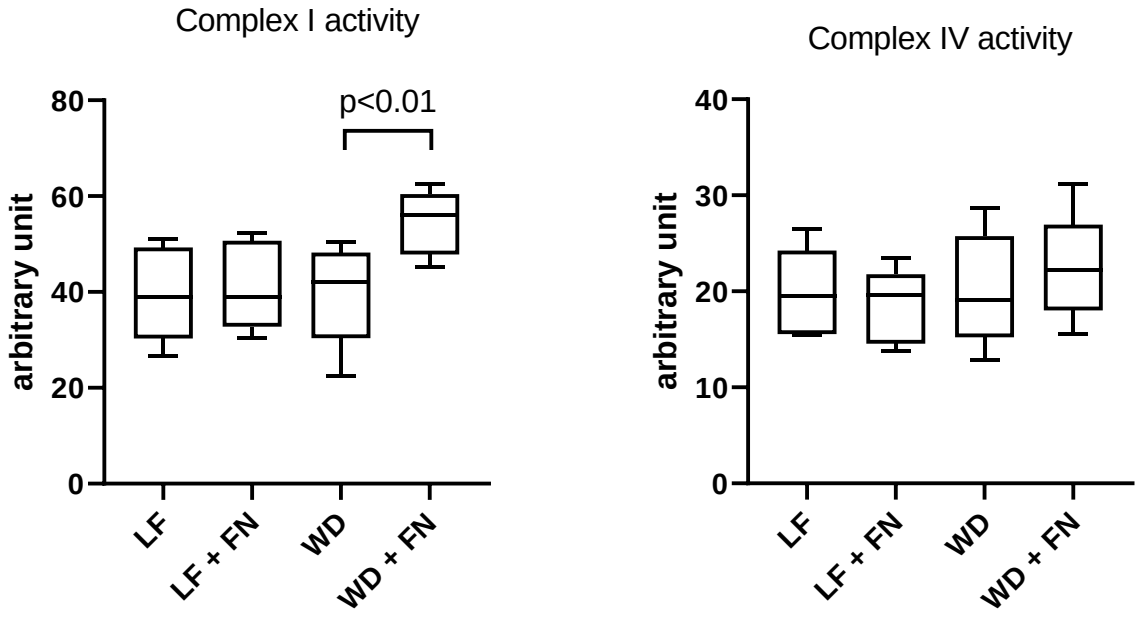
Complex I activity
p<0.01
arbitrary unit
80
60
40
20
0
LF
LF + FN
WD
WD + FN
Complex IV activity
arbitrary unit
40
30
20
10
0
LF
LF + FN
WD
WD + FN

Figure 6

E

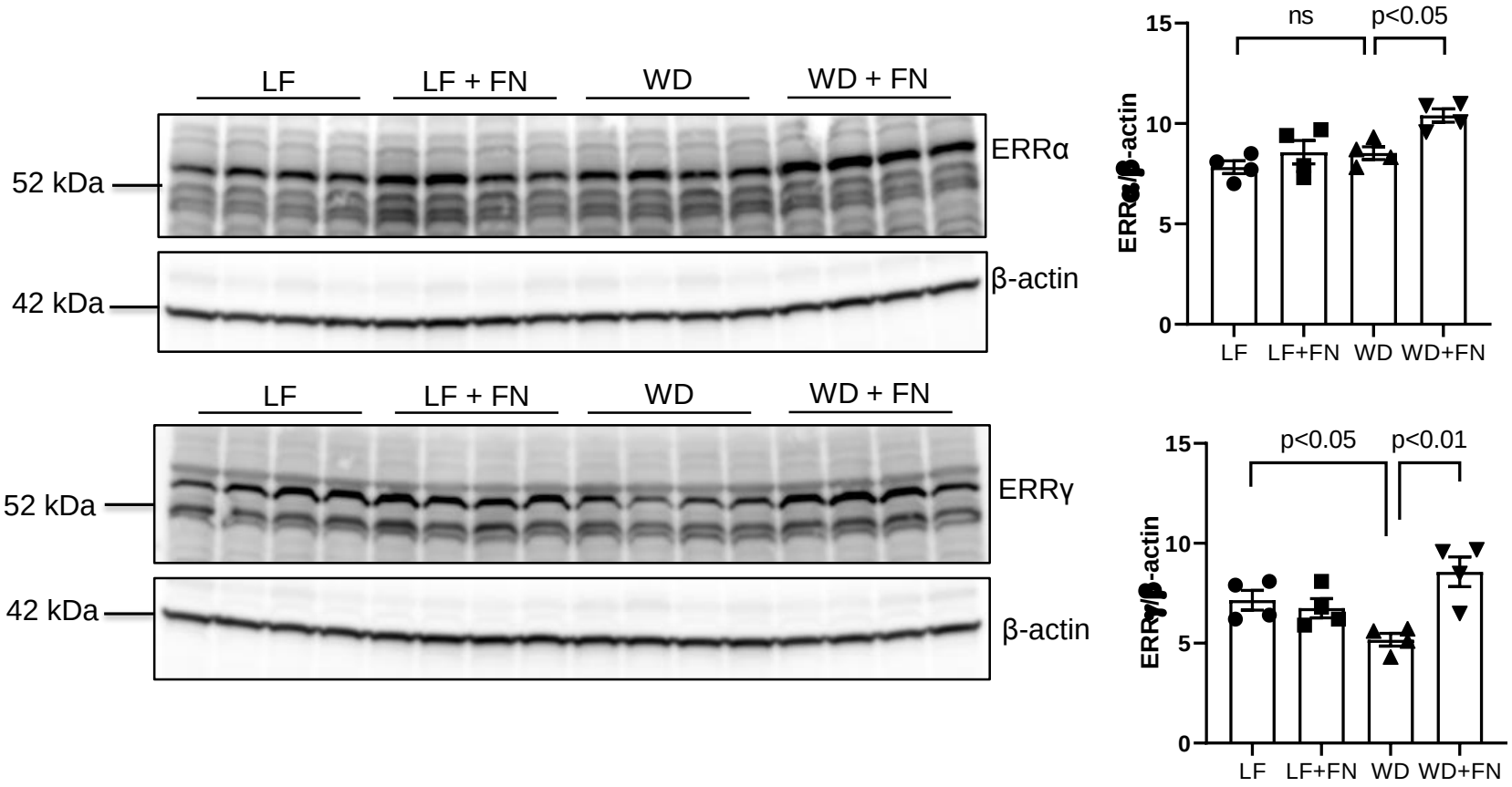
LF
LF + FN
WD
WD + FN
52 kDa
42 kDa
ERRα
β-actin
ns
p<0.05
ERRα/β-actin
15
10
5
0
LF
LF+FN
WD
WD+FN
LF
LF + FN
WD
WD + FN
52 kDa
42 kDa
ERRγ
β-actin
p<0.05
p<0.01
ERRγ/β-actin
15
10
5
0
LF
LF+FN
WD
WD+FN

Figure 6

F

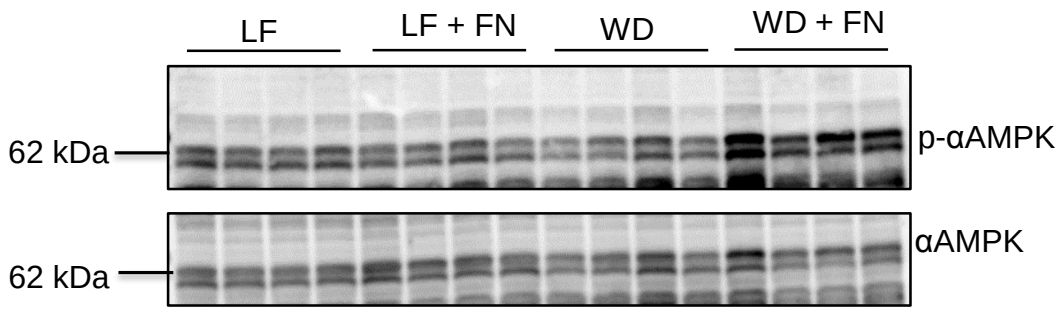
LF
LF + FN
WD
WD + FN
62 kDa
p-αAMPK
62 kDa
αAMPK

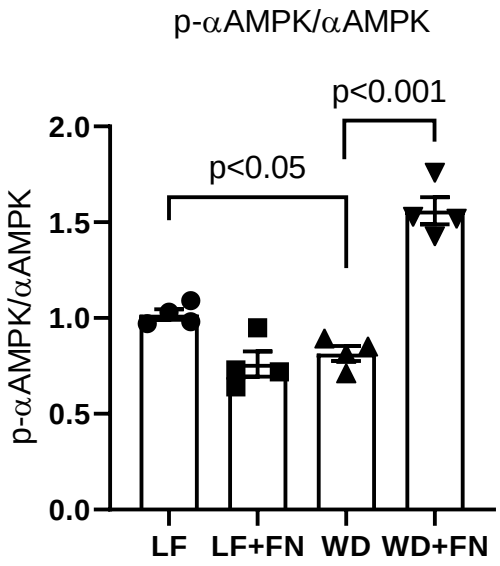
p-αAMPK/αAMPK
p<0.001
p<0.05
2.0
1.5
1.0
0.5
0.0
p-αAMPK/αAMPK
LF
LF+FN
WD
WD+FN

Supplementary Figure 1

A

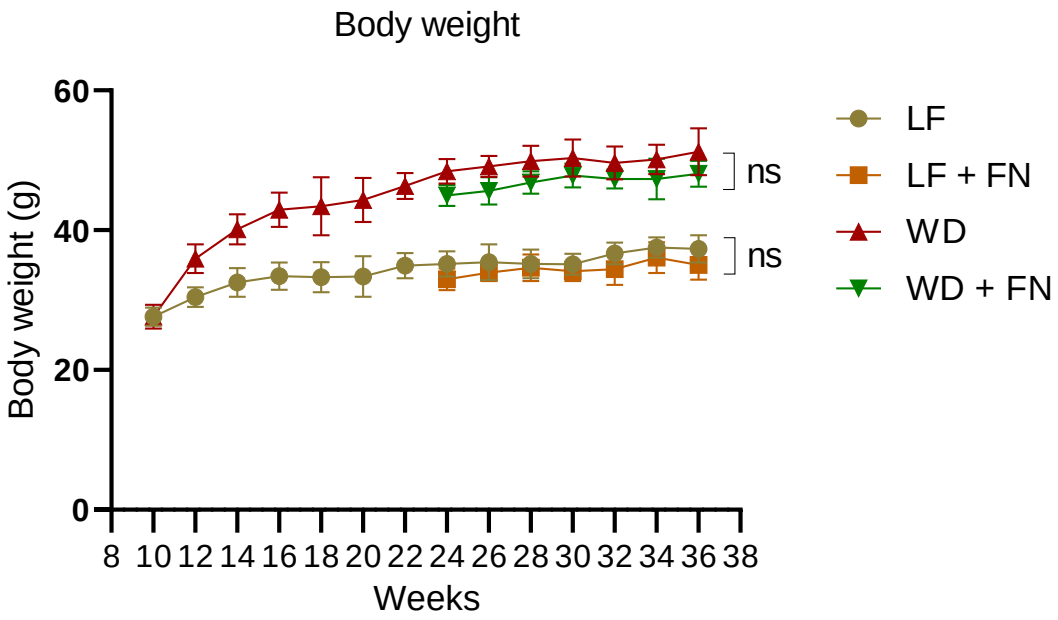

Supplementary Figure 1

B

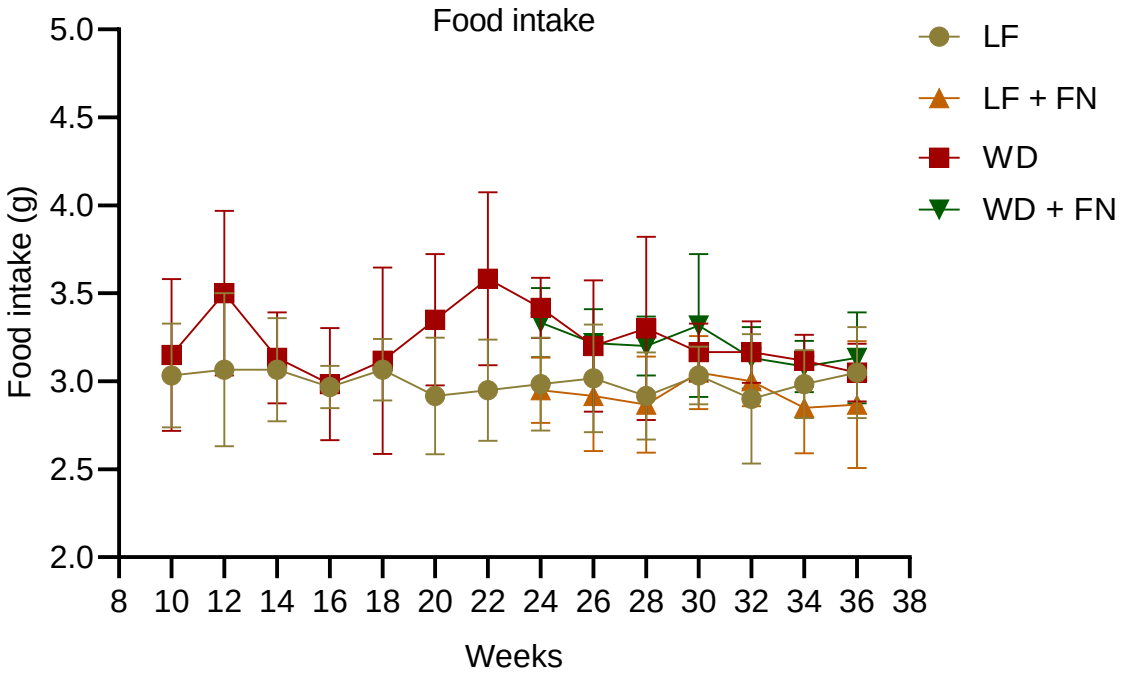

Supplementary Table

Gene name	Forward	Reverse
Fn1	ATGTGGACCCCTCCTGATAGT	GCCCAGTGATTTCAGCAAAGG
Col4a2	GACCGAGTGCGGTTCAAAG	CGCAGGGCACATCCAACTT
Pai1	GACTCTGGATGAGTGGAAAGC	GGCGGCCTAAGTCTCCAAAAT
TGFb	CTCCCGTGGCTTCTAGTGC	GCCTTAGTTTGGACAGGATCTG
CTGF	GGGCCTCTTCTGCGATTTC	ATCCAGGCAAGTGCATTGGTA
Timp1	GCAACTCGGACCTGGTCATAA	CGGCCCGTGATGAGAAACT
MCP1	TTAAAAACCTGGATCGGAACCAA	GCATTAGCTTCAGATTTACGGGT
NLRP3	GCCTTGAAGAAGAGTGGATGG	GCGTGTAGCGACTGTTGAG
cGAS	GAGGCGCGGAAAGTCGTAA	TTGTCCGGTTCCTTCCTGGA
TMEM173	GGTCACCGCTCCAAATATGTAG	CAGTAGTCCAAGTTCGTGCGA
TLR2	GCAAACGCTGTTCTGCTCAG	AGGCGTCTCCCTCTATTGTATT